

This discussion paper is/has been under review for the journal *Atmospheric Chemistry and Physics (ACP)*. Please refer to the corresponding final paper in *ACP* if available.

# Particle number size distributions in urban air before and after volatilisation

W. Birmili<sup>1</sup>, K. Heinke<sup>1,2</sup>, M. Pitz<sup>3,4</sup>, J. Matschullat<sup>2</sup>, A. Wiedensohler<sup>1</sup>,  
J. Cyrys<sup>3,4</sup>, H.-E. Wichmann<sup>3</sup>, and A. Peters<sup>3</sup>

<sup>1</sup>Leibniz Institute for Tropospheric Research (IfT), Permoserstrasse 15,  
04318 Leipzig, Germany

<sup>2</sup>Interdisciplinary Environmental Research Centre (IÖZ), TU Bergakademie Freiberg, 09599  
Freiberg, Germany

<sup>3</sup>Helmholtz Zentrum München (HMGU), German Research Center for Environment Health,  
Institute of Epidemiology, 85758 Neuherberg/Munich, Germany

<sup>4</sup>University of Augsburg, Center for Science and Environment, 86159 Augsburg, Germany

Received: 25 February 2009 – Accepted: 30 March 2009 – Published: 7 April 2009

Correspondence to: W. Birmili (birmili@tropos.de)

Published by Copernicus Publications on behalf of the European Geosciences Union.

## Size distributions before and after volatilisation

W. Birmili et al.

Title Page

Abstract

Introduction

Conclusions

References

Tables

Figures

◀

▶

◀

▶

Back

Close

Full Screen / Esc

Printer-friendly Version

Interactive Discussion

## Abstract

Aerosol particle number size distributions (size range 0.003–10  $\mu\text{m}$ ) with and without using a thermodenuder are measured continuously in the city of Augsburg, Germany. Here, the data between 2004 and 2006 are examined with respect to the governing anthropogenic sources and meteorological factors. The two-year average particle number concentration in Augsburg was found to be 12 200  $\text{cm}^{-3}$ , similar to previous observations in other European cities. A seasonal analysis yielded twice the total particle number concentrations in winter as compared to summer, a consequence of more frequent inversion situations and particulate emissions in winter. The diurnal variation of the size distribution is shaped by a remarkable increase in the morning along with the peak traffic hours. After a mid-day decrease along with the onset of vertical mixing, an evening increase in concentration could frequently be observed, suggesting a re-stratification of the urban atmosphere. The mixed layer height turned out to be the most influential meteorological parameter on particle size distribution. Its influence was greater than that of the geographical origin of the synoptic-scale air masses.

By heating every second aerosol sample to 300°C in a thermodenuder, the volume fraction of non-volatile compounds in the urban aerosol was retrieved. The obtained results compared well with an independent measurement of the aerosol absorption coefficient ( $R^2=0.9$ ). The balance of particle number upstream and downstream of the thermodenuder suggests that all particles >12 nm contain a non-volatile core at 300°C. As an artefact of the volatility analysis, nucleation of particles smaller than 6 nm was observed in the cooling section of the thermodenuder. An average diameter ratio of particles before and after volatilisation was determined as a function of particle size. It indicated that particles >60 nm contain significantly higher fractions of non-volatile compounds, most likely soot, than particles <60 nm.

### Size distributions before and after volatilisation

W. Birmili et al.

Title Page

Abstract

Introduction

Conclusions

References

Tables

Figures

◀

▶

◀

▶

Back

Close

Full Screen / Esc

Printer-friendly Version

Interactive Discussion



## 1 Introduction

Atmospheric particles (particulate matter, PM), particularly such of anthropogenic origin, have been shown to cause adverse health effects in humans (Pope and Dockery, 2006; WHO, 2004, 2006). To reduce the number of premature deaths and disease caused by particulate air pollution, legal limit values have been implemented in the European Union, thus regulating the total mass concentration of particles with diameter less than 10  $\mu\text{m}$  (EC, 1999).

Meanwhile, it has become clear that the health risk due to inhalation of environmental particles is most probably not an effect of the total particle mass but of a combination of specific, more toxic sub-fractions of the atmospheric aerosol (HEI, 2002; Sioutas et al., 2005). Identification of the more hazardous sub-fractions of the aerosol would permit reduction measures beneficial for public health. Moreover, legal measures to reduce ambient PM levels could be designed more cost-effective since they would be targetted on the reduction of specific particle types rather than total PM mass.

Several particle types have been proposed to be associated with adverse health effects. Ultrafine particles (UFPs, diameter <100 nm) have been suggested to act more toxically after inhalation than bigger particles (Wichmann and Peters, 2000; von Klot et al., 2005; Oberdörster et al., 2005). Due to their small size, UFPs can penetrate more deeply into the alveolar region, and also contain a higher mass-specific particle surface area, where particles interact with the lung fluid. Other arguments point to the overwhelming carbonaceous character of atmospheric UFPs: Insoluble UFPs, such as originating from anthropogenic high-temperature combustion, have a high possibility to deposit in alveolar spaces and subsequently translocate into their interstitial spaces and later to other organ systems (Möller et al., 2008). A link to respiratory and cardiovascular disease has been suggested (Kreyling and Scheuch, 2000; Schwarze et al., 2006). Other reported risk factors are related to the biological surface reactivity, as well as specific (bio-)chemical compounds as distinct as transition metals and endotoxins. Concluding from the above discussion, a more specific physical and chemical aerosol

### Size distributions before and after volatilisation

W. Birmili et al.

Title Page

Abstract

Introduction

Conclusions

References

Tables

Figures

◀

▶

◀

▶

Back

Close

Full Screen / Esc

Printer-friendly Version

Interactive Discussion



characterisation would be desirable for both, specialised health-related studies as well as government monitoring networks.

One useful parameter is the particle number size distribution, from which various parameters such as the number of ultrafine particles as well as the particle surface area may be derived. Long-term measurements of ambient particle size distributions have been scarce until recently, but the body of reports on such measurements is augmenting. Ambient size distribution measurements have revealed that the engine exhaust of motor vehicles causes enormous numbers of particles near urban roads (Hitchins et al., 2000; Wehner et al., 2002a; Charron and Harrison, 2003; Ketzel et al., 2003; Zhu et al., 2004; Voigtländer et al., 2006) as well as motorways (Zhu et al., 2004; Rosenbohm et al., 2005; Imhof et al., 2005). In cities where traffic is the dominating source of anthropogenic particles, the particle size distribution at urban background sites shows an attenuated image of the daily traffic cycle (Ebelt et al., 2001; Kreyling et al., 2003; Wehner and Wiedensohler, 2003; van Dingenen et al., 2004; Hussein et al., 2004; Ketzel et al., 2004; Aalto et al., 2005). In the presence of solar radiation, the total particle number in urban areas is also influenced by photochemically-induced secondary formation (Kulmala et al., 2004; Costabile et al., 2008).

Volatility analysis (thermal discrimination) is a technique to remove the more volatile species of the particles at a prescribed temperature (Schmid et al., 2002). Thermodenuders separate volatile from non-volatile compounds while the particles remain in the airborne state (Burtscher et al., 2001). The design of thermodenuders has been improved with respect to efficient vapour removal (Wehner et al., 2002b; Fierz et al., 2007), short transit time (An et al., 2007), and rapid response towards temperature changes (Huffman et al., 2008).

Particulate emissions of diesel vehicles exhibit a soot particle mode with diameters around 80 nm, and a smaller nucleation mode originating from recondensation of unburnt fuels (Ntziachristos et al., 2004). While the diesel soot mode is rather non-volatile at temperatures of 300°C, the condensation mode is composed mainly of long-chained organics volatile above 100°C (Sakurai et al., 2003).

## Size distributions before and after volatilisation

W. Birmili et al.

Title Page

Abstract

Introduction

Conclusions

References

Tables

Figures

◀

▶

◀

▶

Back

Close

Full Screen / Esc

Printer-friendly Version

Interactive Discussion



**Size distributions  
before and after  
volatilisation**

W. Birmili et al.

Title Page

Abstract

Introduction

Conclusions

References

Tables

Figures

◀

▶

◀

▶

Back

Close

Full Screen / Esc

Printer-friendly Version

Interactive Discussion

Measurements with volatility analysers (Philippin et al., 2004; Rose et al., 2006) or  
thermodenuders in conjunction with particle mobility spectrometers (Hasegawa et al.,  
2004) have confirmed the ubiquity of traffic-derived soot particles in the proximity of  
highly trafficked roads. In a street canyon in Leipzig, for example, the number frac-  
5 tion of externally mixed soot particles was concluded to amount to 60% compared to  
6% at a rural reference station (Rose et al., 2006). Besides, thermodenuder/mobility  
spectrometer combinations have also been used to examine nucleation mode particles  
evolving from photochemically-induced secondary formation (Wehner et al., 2005; Ehn  
et al., 2007). The latter works suggested that even freshly formed particles contain a  
10 core that is non-volatile at 300°C.

The aim of this work was to quantify and discuss particle number size distributions  
and their non-volatile cores in the city of Augsburg, southern Germany. The particu-  
lar interest in Augsburg derives from the interdisciplinary research platform KORA  
(*Kooperative Gesundheitsforschung in der Region Augsburg* – cooperative health re-  
15 search in the Augsburg region), which was established already in 1984 (Holle et al.,  
2005). A comprehensive body of epidemiological studies within KORA has suggested  
a link between air pollution and cardiovascular diseases, but also revealed the need  
of a more detailed characterization of air pollutants, notably the physical and chemical  
properties of airborne particles and their temporal variability (Peters et al., 2005; von  
20 Klot et al., 2005). Within KORA, particular efforts are directed towards identifying the  
health-relevant sub-fractions in the ambient aerosol.

Our study pursues a statistical characterisation of two years of particle size distribu-  
tion observations (3–10 000 nm) in the urban atmosphere of Augsburg. Size distribution  
measurements downstream of a thermodenuder allow conclusions on the non-volatile  
25 sub-fraction in sub- $\mu\text{m}$ , which is broadly associated with soot. Using local meteorologi-  
cal parameters as well as back trajectory calculations, the study provides an analysis of  
the climatologically relevant processes that control the environmental aerosol in Aug-  
sburg.

## 2 Experimental

### 2.1 Sampling site

In November 2004, the Helmholtz Zentrum München (HMGU) started particle number size distribution measurements at an urban background monitoring station in Augsburg. The HMGU monitoring station is located at an urban background setting on premises of Augsburg's University of Applied Sciences (Fachhochschule Augsburg) (48° 22' N; 10° 54' E). The station is located about 1 km south of Augsburg's city centre with the nearest street being about 100 m north-east of the site (Fig. 1). Spatially resolved measurements of total particle number suggested this site of being representative of urban background conditions (Cyrus et al., 2008). Pitz et al. (2008a) reported additional details of the site.

### 2.2 Instrumentation

Particle number size distributions in a diameter ( $D_p$ ) range 3–800 nm were measured using a flow-regulated twin differential mobility particle sizer (TDMPS). This instrument is based on two differential mobility analysers covering complementary size ranges (Birmili et al., 1999). Briefly, the first subsystem combines an ultrafine Vienna-type differential mobility analyzer (electrode length 11 cm) with an ultrafine condensation particle counter (UCPC model 3025, TSI Inc., Shoreview, USA) to measure particles across a range from 3 to 23 nm. The second subsystem combines another differential mobility analyzer (electrode length 28 cm) with a condensation particle counter (CPC model 3010, TSI Inc.) to measure particles between 18 and 800 nm. The sheath air is circulated in a closed loop, at relative humidities ranging mostly between 10 and 30%.

Upstream the TDMPS, a thermodenuder (TD) was deployed as an option to remove volatile aerosol components. The thermodenuder follows the design of Wehner et al. (2002b), where volatile particle material is evaporated at a temperature of 300°C, and subsequently removed with the assistance of active carbon in a cooling section. The

## Size distributions before and after volatilisation

W. Birmili et al.

Title Page

Abstract

Introduction

Conclusions

References

Tables

Figures

⏪

⏩

◀

▶

Back

Close

Full Screen / Esc

Printer-friendly Version

Interactive Discussion



temperature of 300°C was selected with the aim of evaporating the overwhelming fraction of inorganic ions (particularly ammonium sulfate and nitrate, although not sodium chloride) as well as organic carbon from the particle phase. On the other hand, 300°C is a temperature at which charring<sup>1</sup> of organic compounds is avoided.

5 The standard operation procedure for the TDMPs was to record size distributions upstream and downstream of the TD in alternating sampling intervals of 10 min (cf. inset in Fig. 1). This procedure provided a steady flow of size distributions both with and without the TD, and an overall time resolution of 20 min for each of these measurement modes. Before further data analysis, the size distribution data was averaged to hourly values.

10 Occasionally, extreme concentrations of particles with diameters less than 6 nm were observed downstream of the TD, which were identified as the re-nucleation of gas-phase species in the cooling section of the TD due to incomplete removal of volatilized material. This operational artifact could not be completely eliminated. Figure 2 gives an illustration of its effect on total particle number concentration. It can be seen that the perturbing effect of the nucleation can be eliminated by truncating the number size distributions downstream of the TD at 10 nm.

15 The instrumentation also contains an aerodynamic particle sizer (APS model 3321, TSI Inc.) which measures aerodynamic size distributions of ambient particles between 0.8 and 10 μm. We refrained from connecting the APS to the TD because of the considerable length of sampling pipe associated with the thermodenuder; this would lead to irreversible sampling losses of the super-μm particles. Gravimetric PM<sub>2.5</sub> and PM<sub>10</sub> mass concentrations were determined using a tapered element oscillating microbalances (TEOM) equipped with a filter dynamics measurement system.

25 Mass concentrations of black carbon (BC) were determined using an aethalometer (Type 8100, Thermo Fisher Scientific Inc.). The aethalometer converts light attenuation through a particle-laden quartz fiber filter into BC mass concentration using the exper-

<sup>1</sup>Charring is the incomplete combustion of (oxygenated) hydrocarbons removing hydrogen and oxygen, and leaving pure carbon.

**Size distributions before and after volatilisation**

W. Birmili et al.

Title Page

Abstract

Introduction

Conclusions

References

Tables

Figures

◀

▶

◀

▶

Back

Close

Full Screen / Esc

Printer-friendly Version

Interactive Discussion



**Size distributions  
before and after  
volatilisation**

W. Birmili et al.

Title Page

Abstract

Introduction

Conclusions

References

Tables

Figures

◀

▶

◀

▶

Back

Close

Full Screen / Esc

Printer-friendly Version

Interactive Discussion



imentally determined specific attenuation cross-section of  $16.6 \text{ m}^2 \text{ g}^{-1}$  at a wavelength of 880 nm. To validate the aethalometer's performance, we compared the instrument during one month in Augsburg against a high quality reference instrument, the multi-angle absorption photometer (MAAP; cf. Sheridan et al., 2005). Our intercomparison suggested that the aethalometer values are biased by a value between +0.26 and +0.32  $\mu\text{g m}^{-3}$  at the zero end, while the mean concentration during the period was matched rather precisely (MAAP:  $1.89 \mu\text{g m}^{-3}$ , aethalometer:  $1.87 \mu\text{g m}^{-3}$ , Spearman rank coefficient 0.98).

Finally, meteorological parameters (wind speed, wind direction, temperature, relative humidity) were collected continuously at the HMGU station, and at a meteorological roof-top station (height: 20 m) of FH Augsburg distant at about 0.5 km. While the winds at the HMGU station tend to be influenced by the surrounding buildings, the winds at the roof-top station can be considered representative for the entire urban area.

### 2.3 Size distribution evaluation

TDMPs size distributions were evaluated according to the detailed description given by Pitz et al. (2008b).

Briefly, the branches of both differential mobility analyser subsystems were assimilated into a single mobility distribution encompassing 3–800 nm. The mobility distributions were converted into size distributions using a multiple charge inversion, taking into account experimentally determined CPC and DMA transfer functions. Diffusional particle losses in the heated TD were corrected by a transmission function obtained by using laboratory-generated silver particles across the size range 3–50 nm. TDMPs and APS size distributions were combined into a single size distribution between 3 and 10 000 nm assuming an effective density of  $1.7 \text{ g cm}^{-3}$  for the conversion of aerodynamic into electromobility diameters. This particular density value reconciles the particle mass concentrations calculated from TDMPs/APS volume size distributions with the gravimetric  $\text{PM}_{10}$  measurement (Pitz et al., 2008b).

## 2.4 Diameter shrinking factors

To relate the size distributions obtained with and without application of the TD, the summation method (SM) was used. This method was originally developed for the analysis of the hygroscopic growth of particle size distributions (Birmili et al., 2009) but has since been applied to quantify the loss in particle diameter after passing through a TD (Engler et al., 2007).

The SM assumes that the particle number size distribution is rearranged as a result of the aerosol conditioning. It associates segments of equal particle number concentration under the conditioned and non-conditioned size distributions – beginning at their upper tail, and continuing downwards. The ratio between the mean diameters of two corresponding particle number segments is the particle diameter shrinking factor (SF hereafter), concretely the fraction of their original diameter onto which particles collapse after passage through the TD. We refer the reader to a previous report (Birmili et al., 2009) for a detailed account of the calculation method.

A first prerequisite of the SM is that the total particle number is conserved during aerosol conditioning. Figure 2 shows the ratio between the respective experimental particle number concentrations downstream and upstream the thermodenuder. Different pairs of lower cut-off diameters (3 and 6 nm, 7 and 14 nm, and 10 and 20 nm) were used to evaluate the sensitivity of this ratio on whether ignoring or not the lowest size channels, i.e. those that are affected by artificial nucleation in the thermodenuder. When ignoring the lowest size channels the particle number balance across the thermodenuder becomes approximately unity.

Figure 2 suggests that total particle number concentration across the thermodenuder in Augsburg is conserved within the accuracy of measurement, as long as only particles with ambient diameter >20 nm are considered. A second prerequisite is that the external mixture of the sampled aerosol varies only slowly with particle diameter. A suitable tool for the verification of SM results is, in particular, the volatility tandem analyser method. In a previous work (Engler et al., 2007) we were able to establish that the

### Size distributions before and after volatilisation

W. Birmili et al.

Title Page

Abstract

Introduction

Conclusions

References

Tables

Figures

◀

▶

◀

▶

Back

Close

Full Screen / Esc

Printer-friendly Version

Interactive Discussion



diameter shrinking factors obtained by the SM indeed correspond to the shrinking behaviour of monodisperse particle populations selected by a volatility tandem analyser.

Limitations of the SM arise due to limited counting statistics at the upper tail of the size distribution, and due to the possibly incomplete recovery of particle losses occurring in the TD. As a consequence of both experiences, we limited the output range of SFs to 30–300 nm. Additional uncertainty derives from the non-simultaneity of the conditioned and non-conditioned size distribution measurements. This uncertainty was alleviated by first, using a buffer volume (20 l) in the aerosol inlet system and second, by averaging size distributions to hourly values before applying the SM.

## 2.5 Determination of the mixed layer height

The mixed layer height (MLH) is the most important single meteorological parameter describing vertical air exchange and pollutant dispersal (Stull, 1988). For an estimate of the MLH we evaluated the nearest regular radiosounding data, recorded daily at 13:00 local time at Munich/Oberschleissheim (50 km east of Augsburg). The MLH was derived from the pseudopotential temperature using the simple parcel method (Holzworth, 1964). The aerosol data in Augsburg were aggregated to a daily average covering the period between 12:00 and 18:00, which captures essentially the daily minimum in Aitken and accumulation particle concentrations (cf. Fig. 5b–e below).

## 2.6 Back trajectory cluster analysis

A k-means cluster analysis combining 3d-back trajectories and vertical temperature profiles was applied to the entire dataset in close analogy to the work of Engler et al. (2007). The inclusion of vertical potential temperature profiles into the cluster analysis proved vital in understanding the reasons for high and low levels of particle number in Augsburg. The cluster algorithm divided the dataset into a predetermined number of 13 trajectory clusters. 6-day back trajectories were calculated for each day 13:00 UTC using the HYSPLIT model on the NOAA AR Ready Website (Draxler and Hess, 2004).

### Size distributions before and after volatilisation

W. Birmili et al.

Title Page

Abstract

Introduction

Conclusions

References

Tables

Figures

◀

▶

◀

▶

Back

Close

Full Screen / Esc

Printer-friendly Version

Interactive Discussion



Particle size distributions were averaged over the time interval 12:00–18:00 LT. According to the minimum concentrations observed in Fig. 5 below, that period represents best a homogeneously mixed boundary layer.

### 3 Results and discussion

#### 3.1 Non-conditioned particle data

##### 3.1.1 Number concentrations and size distributions

Figure 3 illustrates the median number and volume distributions in Augsburg for the entire 2-year period. The number distribution of particles upstream of the thermodenuder (TD) features a single maximum in the Aitken mode ( $\sim 40$  nm), while the volume size distribution shows two peaks that mark the accumulation and coarse particle modes. The latter two modes are separated by a clear minimum around  $1 \mu\text{m}$ . The passage through the TD modifies both distributions, and is discussed in detail in Sect. 3.2.

For a more accessible version of the data, the size distributions were integrated over six diameter intervals (see Table 1). It is worth to note that the boundaries of integration (3, 10, 30, 300, 800, 2000, 10 000 nm) were chosen so that particle populations of a maximum statistical independence were generated (cf. auto-correlation analysis below).

The mean particle number concentration in Augsburg was  $12\,000 \text{ cm}^{-3}$  for the size range 3–10 000 nm and the biennial period (sum of  $\mu$  in Table 1), with the size interval 30–300 nm encompassing the majority of total particle number ( $7600 \text{ cm}^{-3}$ ). The observed numbers are comparable with former observations of total particle number in Augsburg (Aalto et al., 2005), and tend to lie in the lower range of worldwide urban background observations ( $5000$ – $50\,000 \text{ cm}^{-3}$ ). We particularly took note of the long-term observations (i.e. covering more than one year) reported for Alkmaar and Erfurt (both  $18\,000 \text{ cm}^{-3}$ ; Ruuskanen et al., 2001), Helsinki ( $16\,000 \text{ cm}^{-3}$ ; Ruuskanen et al.,

Title Page

Abstract

Introduction

Conclusions

References

Tables

Figures

◀

▶

◀

▶

Back

Close

Full Screen / Esc

Printer-friendly Version

Interactive Discussion



2001), Leipzig (16 000 cm<sup>-3</sup>; Wehner and Wiedensohler, 2003), Copenhagen (7000 and 24 000 cm<sup>-3</sup>; Ketzler et al., 2004), Pittsburgh (22 000 cm<sup>-3</sup>; Stanier et al., 2004), Atlanta (21 000 cm<sup>-3</sup>; Woo et al., 2001), and Beijing (33 000 cm<sup>-3</sup>; Wehner et al., 2008).

### 3.1.2 Annual cycle

5 Annual cycles of environmental parameters are useful to examine the effect of seasonal changes, such as of temperature, relative humidity, and also the activity of natural and anthropogenic particle sources. Figure 4 presents particle number concentrations for six discrete particle diameters (7, 30, 80, 275, 600, and 2000 nm). Similarly to Sect. 3.1.1 the diameters were selected so that statistically independent particle populations are represented. In addition, the time series were normalized to an average of unity, and smoothed by a running 30-day median.

15 Figure 4 highlights the occurrence of high number concentrations during enduring periods with cold ambient temperatures. A closer look at the time series – shown in detail in Fig. 15 in the appendix, revealed that the high particle concentrations were associated with several cold periods, where temperatures fell particularly low. These were, in detail, 16–19 January, 2005 (day 381–384): minimum temperature –7.8°C; 28–31 January 2005 (day 393–396): –12.2°C; 5–9 February 2005 (day 401–405): –11.7°C; 22–28 February 2005 (day 418–424): –11.9°C; 3–5 March 2005 (day 427–429): –12.5°C; 10–16 January 2006 (day 740–746): –10.4°C; 23 January–2 February 2006 (day 753–765): –12.4°C. It is mainly these episodes which lead to a substantial difference in average total particle number between winter (December, January, February; 15 000 cm<sup>-3</sup>) and summer (June, July, August; 10 000 cm<sup>-3</sup>).

25 The enhanced concentrations in winter are attributed to two effects: Additional particulate emissions from domestic heating and power generation and second, less pronounced vertical mixing of the atmosphere. Both effects are particularly the consequence of very cold temperatures. Such an annual cycle is not unusual but has been observed in other urban size distribution data sets in the Northern hemisphere before

## Size distributions before and after volatilisation

W. Birmili et al.

Title Page

Abstract

Introduction

Conclusions

References

Tables

Figures

◀

▶

◀

▶

Back

Close

Full Screen / Esc

Printer-friendly Version

Interactive Discussion



(Wichmann et al., 2002; Wehner and Wiedensohler, 2003; Hussein et al., 2004; Aalto et al., 2005).

We observed that the concentrations of 7 nm particles showed a similar annual cycle as the rest of the sub- $\mu\text{m}$  particles. Atmospheric particle formation events as a result of photochemical processes were only rarely observed in Augsburg, even during the warm season. Thus, the new particle formation events have no significance for the annual cycle in Fig. 4.

It is an essential observation that the concentrations of coarse particles (2000 nm) show the reverse behaviour, with summer averages being higher by 50% compared to winter. We see this as evidence for an increased probability of particle re-suspension from agricultural lands and roads in summer. The remarkable correlation between coarse particle concentrations and temperature (Fig. 4) suggests dried out surfaces as the prime reason for increased re-suspension.

### 3.1.3 Diurnal cycle

Figure 5 gives diurnal cycles of the particle number concentrations at the six previously selected diameters. The data are distinguished between weekdays (Monday–Thursday), Saturdays and Sundays. At all particle diameters the concentrations reveal a maximum during the morning peak traffic period (06:00–09:00 LT). Its occurrence in all particle diameters suggests a broad impact of traffic emissions on the entire particle size spectrum. The relative magnitude of this morning peak is the greatest for the lowest particle diameters 7, 30 and 80 nm. While the latter particle diameters are in particular indicative of exhaust emissions, coarse particles – represented by the 2000 nm diameter in Fig. 5f, have rather been associated with direct sources due to abrasion and vehicle-induced re-suspension (Thorpe and Harrison, 2008).

The particle concentrations at all diameters decreased steadily as of 08:00 towards noon. This re-occurring feature is ascribed to the dilution of the emitted pollutants in an increasingly well-mixed boundary layer rather than changes in traffic density, the latter remaining rather constant throughout the daylight hours. The morning peak turns

## Size distributions before and after volatilisation

W. Birmili et al.

Title Page

Abstract

Introduction

Conclusions

References

Tables

Figures

◀

▶

◀

▶

Back

Close

Full Screen / Esc

Printer-friendly Version

Interactive Discussion



out considerably lower on Saturdays, and is entirely missing on Sundays as a result of lower traffic densities at that time of day.

For the particle diameters 30, 80, 275 and 600 nm, concentrations show a second maximum in the evening (20:00–24:00 LT) as well. We suspect that this second maximum is the result of pollution trapping, since it coincides with the time of re-stratification in the urban atmosphere rather than any increase in traffic. The observations shown highlight the relevance of urban traffic emissions on the HMGU station in Augsburg, similar to comparable observations at urban background locations in German cities of comparable size (Wehner and Wiedensohler, 2003; Cyrys et al., 2003).

### 3.1.4 Auto-correlation analysis

The time fluctuations of the size distribution data were more closely examined by calculating the autocorrelation function (ACF). Figure 6 shows the ACF for five selected size channels (10, 50, 120, 600, and 5000 nm). The ACF of 10 and 50 nm particles decreases rapidly with lag time, indicating a low persistence of their concentrations in the urban atmosphere. However, their concentrations exhibit a significant diurnal autocorrelation, manifested by local maxima in the ACF at multiples of 1 d.

When passing over to larger particles, the diurnal autocorrelation becomes less significant, at the benefit of a slower decrease of the ACF with the lag time, indicating a higher persistence of the concentrations. The diurnal autocorrelation reappears as a sinusoidal signal in the coarse particle mode (5000 nm), indicating the activity of coarse particle sources on a diurnal scale.

The time variations were analysed more systematically by splitting the ACF into different components by a least-square fit. Four component functions were fitted:  $F_A$ , a decreasing exponential curve representing the persistent (long-lasting) component;  $F_B$ , a sinusoidal curve with period time 1 d representing the daily periodical component;  $F_C$ , a sinusoidal curve with period time 7 d representing the weekly periodical component;  $F_D$ , an additional constant used for achieving a better numerical fit. Figure 7 shows the integrals values over  $F_A$ ,  $F_B$ , and  $F_C$  as a function of particle size.

## Size distributions before and after volatilisation

W. Birmili et al.

Title Page

Abstract

Introduction

Conclusions

References

Tables

Figures



Back

Close

Full Screen / Esc

Printer-friendly Version

Interactive Discussion



---

**Size distributions  
before and after  
volatilisation**W. Birmili et al.

---

[Title Page](#)[Abstract](#)[Introduction](#)[Conclusions](#)[References](#)[Tables](#)[Figures](#)[⏪](#)[⏩](#)[◀](#)[▶](#)[Back](#)[Close](#)[Full Screen / Esc](#)[Printer-friendly Version](#)[Interactive Discussion](#)

As indicated in Fig. 6 before, the persistent component  $F_A$  was found to be dominant between 100 and 5000 nm, peaking at 600 nm. This confirms the accumulation mode and the lower part of the coarse particle mode as the long-lasting aerosol components at the HMGU station in Augsburg: The concentrations in the size range 100–5000 nm change only slowly; they are determined by atmospheric processes lasting a few days and longer.

The diurnal component  $F_B$ , in contrast, was dominant in the size range <10 nm and showed non-negligible contributions >2000 nm. In the size range <10 nm, this points to daily variations of newly formed particles as a result of photochemical processes along with solar radiation, while in the coarse mode it indicates the activity of abrasion and re-suspension sources. Finally, the weekly periodic component  $F_C$  shows a maximum at 20 nm and a minor maximum in the coarse mode. The weekly component reflects, in any case, co-variations over 7 days and therefore represents the intensity of anthropogenic contributions.

In conclusion, the particle number concentration between 3 and 10 nm seems to originate overwhelmingly from photochemical processes, that between 10 to 30 nm mainly from the exhaust of motor vehicles. Particles in the range 30 to 300 nm show a strong signature of area-wide particulate emissions, while particles between 300 and 800 nm represent long-range transport (cf. Costabile et al., 2008). Particles in the intervals 0.8–2.0  $\mu\text{m}$  and 2–10  $\mu\text{m}$  are also thought to originate substantially from local and regional emissions, such as direct vehicle emissions, vehicle-induced re-suspension, but also wind-blown dust.

## 3.2 Particle data after volatilisation at 300°C

### 3.2.1 Number concentrations and size distributions

The passage through the TD modifies the original particle size spectrum (Fig. 3). While thermal conditioning kept the total particle number constant within the accuracy of the measurement (see also Fig. 2), its effect on total particle volume was more significant:

69% of the particulate volume ( $D_p < 800$  nm) was removed by the TD, leaving a non-volatile volume fraction of 31%.

In contrast to the monomodal size distribution of non-conditioned particles, the distribution of non-volatile residuals exhibited two peaks around 10 and 70 nm, respectively (Fig. 3). We explain this transformation from a monomodal into a bimodal distribution by the presence of an external particle mixture: First, a sub-population of nearly non-volatile particles exists, which remains at roughly their original size. Second, a population of partly volatile particles exist, which shrink to a small fraction of their original size. Earlier volatility analyser measurements in Leipzig suggested that these two populations are relatively well separated, i.e. very few particles show a transitional behaviour between these two particle types (Rose et al., 2006). The latter authors also suggested the non-volatile mode around 70 nm to represent direct vehicular soot emissions, which is plausible in view of the characteristics of soot particles detected in diesel exhaust (Sakurai et al., 2003; Ntziachristos et al., 2004; Kittelson et al., 2006). One might argue that crustal material (e.g. silicates) originating from re-suspension might interfere with the primary soot particles in the thermodenuder measurements. An electron microscopic study in the urban atmosphere of Frankfurt (Germany), however, rejected that argument by identifying the overwhelming majority of urban particles around 100 nm as soot, and not crustal material (Vester et al., 2007).

In contrast to the diesel soot mode, there is much less knowledge about the nature of particles the non-volatile mode around 10 nm observed in Augsburg (Fig. 3). While it seems evident that they are the residuals of bigger, partly volatile particles, the chemical composition of their residuals is unknown. Both Wehner et al. (2005) and Ehn et al. (2007) found that even particles  $< 20$  nm originating from photochemically-induced nucleation, i.e. particles that were at maximum a few hours old, contained a core that was non-volatile at  $300^\circ\text{C}$ . In view of these results it appears necessary to assume that relatively rapid chemical conversions take place within the particle phase, thereby generating thermally resistant compounds. The photooxidation of aromatic compounds in a reaction chamber gave evidence for the generation of thermally resistant polymers

## Size distributions before and after volatilisation

W. Birmili et al.

Title Page

Abstract

Introduction

Conclusions

References

Tables

Figures

◀

▶

◀

▶

Back

Close

Full Screen / Esc

Printer-friendly Version

Interactive Discussion



(Kalberer et al., 2004) but it is unclear to what extent the described processes apply in the real urban atmosphere.

### 3.2.2 Size-dependent shrinking factors

SF indicates the diameter fraction onto which the average particle population of a given size collapses after passing through the TD. Fig. 8 shows SF as a function of particle diameter for the morning peak hours (06:00–09:00), i.e. when the contribution of fresh anthropogenic aerosol was the highest.

The SF values rise continuously from 30 to about 100 nm. Low values between 0.4 and 0.5 at 30 nm, indicate relatively low volume fractions of non-volatile material (ca. 10%). Conversely, this indicates higher volume fractions of volatile species (ca. 90%), among which we presume organic compounds from direct vehicle exhaust emissions but also secondary processes. Between 70 and 120 nm, a relative maximum in SF and thus the non-volatile fraction is reached (Fig. 8). This maximum coincides with the size range of diesel emissions as discussed before. An intermediate minimum around 200 nm indicates an increasing trend in the volatile fraction while the non-volatile fraction grows slowly again towards 300 nm.

Although the size-segregated trends above 100 nm are on the borderline of significance, they might plausibly be explained by liquid phase-production of soluble material during the processing of particles in non-precipitating cloud, which is most relevant just above the activation size of cloud condensation nuclei (~ 100 nm). The second, slightly increasing trend towards 300 nm would be consistent with a growing importance of crustal material with increasing particle size, such as demonstrated, e.g. in Vester et al. (2007).

The greatest overall SF values (~0.7) – indicating a maximum of non-volatile material, were observed during autumn. The 24 h-average SFs of particles between 30 and 300 nm ranged between 0.45 and 0.70 in Augsburg while observations at a rural site in East Germany (Melpitz) yielded average values between 0.35 and 0.55 (Engler et al., 2007). The corresponding non-volatile volume fractions are 0.09–0.34 in Augsburg

## Size distributions before and after volatilisation

W. Birmili et al.

Title Page

Abstract

Introduction

Conclusions

References

Tables

Figures

◀

▶

◀

▶

Back

Close

Full Screen / Esc

Printer-friendly Version

Interactive Discussion



burg and 0.04–0.17 in Melpitz. Thus, non-volatile particle material is enriched in urban background PM in Augsburg by a factor of two compared to the rural background atmosphere (Melpitz). This observation is of relevance for the assessment of particle exposure caused by non-volatile particulate carbon.

### 3.2.3 Diurnal cycles of SF

Figure 9 shows the diurnal cycles of SF for the particle sizes 80 and 30 nm. These populations are remarkable with respect to their relatively high and low fractions of non-volatile particle material (Fig. 8). The diurnal cycle of SF ( $D_p=80$  nm) exhibits a pronounced morning maximum at 08:00, in close analogy to the particle number concentration upstream of the TD (Fig. 6). This reflects, again, enhanced traffic emissions as well as a stratified boundary layer in the morning hours. The corresponding non-volatile volume fractions at 08:00 are 0.37 on weekdays, and 0.19 on Sundays. Combining this information with the rough doubling of particle concentrations from Sundays to weekdays at the mass-dominating particle diameters 275 and 600 nm (Fig. 5d–e) leads to the conclusion that up to 50% of the non-volatile particle volume in the urban background of Augsburg can stem from traffic within the city itself.

For SF ( $D_p=30$  nm) the case is rather different (Fig. 9). Here, the morning peak was missing on weekdays as well as on weekends. Instead, SF shows a consistent minimum during the morning rush hour period (06:00–09:00). Moreover, SF tends to show lower overall values on weekdays compared to weekends. Two conclusions can be drawn here: First, urban 30 nm particles contain considerably less non-volatile material than 80 nm particles, as found already in the above section. Second, traffic-derived 30 nm particles contain a disproportionate (smaller) fraction of non-volatile material, as opposed to 80 nm particles. The latter conclusion is consistent with the observed high volatility of traffic-derived condensation particles (Sakurai et al., 2003). The observations in Fig. 9 highlight the possibility of the TDMPS/TD method to quantify the influence of traffic-derived particles on the mixture of particle types at an urban background site.

## Size distributions before and after volatilisation

W. Birmili et al.

Title Page

Abstract

Introduction

Conclusions

References

Tables

Figures

◀

▶

◀

▶

Back

Close

Full Screen / Esc

Printer-friendly Version

Interactive Discussion



### 3.2.4 Non-volatile particle volume vs. black carbon concentration

In Augsburg, the gravimetric  $PM_{2.5}$  and  $PM_{10}$  mass concentrations correlate highly with the mass concentrations calculated from the combined TDMPs/APS number size distributions (Pitz et al., 2008b). Here, we took the opportunity to examine the correlation between the non-volatile volume concentration ( $D_p < 800$  nm) and the black carbon (BC) mass concentration, determined for  $PM_{2.5}$  using the aethalometer. It is worth mentioning that the upper size cut-offs of both methods are different. However, the size range  $< 800$  nm encompasses the majority 90% of the  $PM_{2.5}$  mass concentration (based on Fig. 3), so the influence of different upper cut-off sizes is assumed to play a minor role only.

The scatter plot between the BC mass concentration and the non-volatile particle volume can be seen in Fig. 10. Linear curves were fitted for each season, with coefficients of determination ( $R^2$ ) of 0.88, 0.93, 0.82 and 0.88 for winter (December–February), autumn (September–November), summer (June–August) and spring (March–May), respectively. Given that black carbon makes up only a sub-fraction of the total PM, the high degree of correlation indicates a close association between the non-volatile and light-absorbing components of PM in Augsburg. It is worth to note that the fit curves shows a positive intercept on the axis of BC. This is very likely caused by the bias that was identified for the readings of the aethalometer in Sect. 2.2.

Based on Fig. 10, one equivalent of non-volatile PM appears to cause more light absorbance in winter compared to summer. The reasons could be differences in the mixing state of the non-volatile PM, and also incorrect assumptions on the sphericity of the particles. Both arguments are likely to be related to the enhanced contributions of soot from domestic heating, power generation, and also traffic in winter. Another explanation, which is hard to verify, could be the presence of absorbing aerosol other than soot during the summer period. Nevertheless, the comparison between both methods suggests that the non-volatile particle volume can be used as a surrogate for the mass concentration of light-absorbing PM, and vice versa.

#### Size distributions before and after volatilisation

W. Birmili et al.

Title Page

Abstract

Introduction

Conclusions

References

Tables

Figures

◀

▶

◀

▶

Back

Close

Full Screen / Esc

Printer-friendly Version

Interactive Discussion



### 3.3 Effects of the mixed layer height

The mixed layer height (MLH) is the most important single meteorological parameter describing vertical air exchange and pollutant dispersal. Low MLHs inhibit the dispersal of the pollutants emitted near the ground, particularly under low wind speeds. Here, we sought for a possible connection between the concentrations of non-volatile particles and the MLH.

Figure 11 shows the relationship between the non-volatile particle volume concentration and the MLH based on the 13:00 radiosoundings. A well-known feature is the prevalence of high MLHs in the summer period; plenty of values exceeded 1500 m. A significant anti-correlation can be seen between the particle volume and the MLH. High non-volatile volume concentrations ( $6\text{--}20\ \mu\text{m}^3\ \text{cm}^{-3}$ ) were observed only for MLHs below 500 m, while concentrations  $>3\ \mu\text{m}^3\ \text{cm}^{-3}$  occurred only for MLHs below 1200 m. Meanwhile, high MLHs above 1300 m led to concentrations mainly below  $2\ \mu\text{m}^3\ \text{cm}^{-3}$ .

It is essential to note that Fig. 11 serves to describe effects of aerosols in Augsburg that are associated with a MLH that is representative for a large area, perhaps a few 100 km but in any case smaller than the synoptic weather scale. We acknowledge that the lack of profiling measurements directly in the city Augsburg might be a constraint of the comparison shown in the figure. Nevertheless, we find our results consistent with the formerly observed dependency of  $\text{PM}_{10}$  on the MLH in various European cities (Kukkonen et al., 2005; Schäfer et al., 2006).

From a public health point of view, it is suggestive that these episodic values of non-volatile particulate volume  $>3\ \mu\text{m}^3\ \text{cm}^{-3}$  (which are associated with soot) would be associated with a higher health risk due to the inhalation of ambient aerosols. It is worth to note that a low MLH does not necessarily imply low particulate volumes: For MLHs  $<500\ \text{m}$ , the majority of particle volumes is below  $2\ \mu\text{m}^3\ \text{cm}^{-3}$ . Thus, other factors, like air mass origin, play a certain confounding role in determining the local particle concentrations.

#### Size distributions before and after volatilisation

W. Birmili et al.

Title Page

Abstract

Introduction

Conclusions

References

Tables

Figures

◀

▶

◀

▶

Back

Close

Full Screen / Esc

Printer-friendly Version

Interactive Discussion

### 3.4 Effects of wind direction and air masses

Wind speed and direction are essential factors in determining local particle concentrations in urban areas. For Augsburg, particle number concentrations were examined as a function of the local wind direction (Fig. 12). For this analysis we used the wind direction of the FH Augsburg roof-top site (cf. Sect. 2.2), which is assumed to be representative for the entire area of Augsburg. The figure suggests only a moderate but systematic dependency of particle concentrations on the local wind direction. Concentrations are systematically lower under westerly winds compared to easterly winds. The lowest concentrations around wind direction  $240^\circ$  coincide with the direction of the statistically highest wind speed. Trafficked roads may be responsible for the peak in 10, 30 and 50 nm concentrations to the north (cf. Fig. 1). Some overall features in Fig. 12 apparently reflect the larger-scale distribution of particle sources. Consequently, these characteristics were examined by back trajectory cluster analysis.

Figure 13 shows the 13 mean back trajectories obtained from k-means cluster analysis. Figure 14 and 14 gives the mean particle size distributions, and Fig. 14 the mean virtual potential temperature profiles obtained from radiosoundings at 13:00 LT. Table 2 describes the mean characteristics of the 13 back trajectories obtained by the cluster algorithm.

Figure 13 shows that the air masses arriving in Augsburg can be classified as either maritime-influenced (wind direction west) or continentally influenced (wind direction east). The particle number distributions in Figure 14 show generally a single maximum between 20 and 50 nm. Due to their small size, these particles are interpreted as being formed over the continent, and eventually within the region of South Germany. Particles bigger than 100 nm, particularly those between 300 and 1000 nm are, in contrast, clearly influenced by larger scale processes, as was evident from the maximum in the persistent auto-correlation component (Fig. 7).

A major observation was that the lowest particle number concentrations in Augsburg were associated with maritime air masses (Cluster Nos. 1, 2, 3, 13). This is consistent

#### Size distributions before and after volatilisation

W. Birmili et al.

Title Page

Abstract

Introduction

Conclusions

References

Tables

Figures

◀

▶

◀

▶

Back

Close

Full Screen / Esc

Printer-friendly Version

Interactive Discussion



---

**Size distributions  
before and after  
volatilisation**W. Birmili et al.

---

[Title Page](#)[Abstract](#)[Introduction](#)[Conclusions](#)[References](#)[Tables](#)[Figures](#)[⏪](#)[⏩](#)[◀](#)[▶](#)[Back](#)[Close](#)[Full Screen / Esc](#)[Printer-friendly Version](#)[Interactive Discussion](#)

with earlier studies at tropospheric background locations (Birmili et al., 2001; Tunved et al., 2003). Surprisingly low number concentrations were observed for two continental clusters (Nos. 6 and 7). A likely reason for these low concentrations is the unusually low vertical stability (Fig. 14) during summer time conditions (Table 2, season index). The trajectory clusters featuring the highest particle number concentrations were Nos. 12, 4 and 8. These clusters are representative of subsiding air from the North Atlantic (No. 12), slow south-westerly air subsiding from the Alps (Nos. 4) and stagnant air over Southern Germany (No. 8). These air masses originate from entirely different large-scale directions. Conversely, trajectory clusters representing continental air masses from Eastern Europe do not belong to those clusters with the highest particle numbers (Nos. 7, 8, 9, 11). The likely reason for the high concentrations associated with the clusters Nos. 12, 4 and 8 is the extraordinary atmospheric stability, with virtual potential temperature gradients between 0.005 and 0.01 K m<sup>-1</sup> in the lowest 500 m of the atmosphere (Fig.14).

It is a main conclusion that the particle size distribution in an urban area such as Augsburg is shaped by a combination of different effects. The vertical stability of the atmosphere, particularly, proved to be a factor more influential than the local or large-scale wind direction. This is worth considering when using the particle data in future epidemiological studies, or particle exposure assessments.

## 4 Conclusions

A comprehensive data set of particle size distributions (0.003–10 μm) was collected between 2004 and 2006 in urban air in Augsburg, Germany. The annual cycle of particle number concentration showed higher total particle number concentrations in winter (15 000 cm<sup>-3</sup>) compared to summer (10 000 cm<sup>-3</sup>), similar to previous observations in European cities. An exception was the concentration of coarse particles (>1 μm) showing a maximum in summer most likely due to enhanced re-suspension. The most extreme particle number concentrations, particularly in the accumulation mode, oc-

curred predominantly during periods of very low temperatures, typically around  $-10^{\circ}\text{C}$ , and are concluded to result from a combination of emissions from heating sources and atmospheric temperature inversion.

Auto-correlation analysis and diurnal profiles showed that the concentrations of ultrafine particles ( $<80\text{ nm}$ ) were dominated by their diurnal and weekly-anthropogenic cycle. While the dominance of the diurnal component for particles  $<10\text{ nm}$  points at the importance of photochemically-induced new particle formation, the existence of a weekly component in the size range  $10\text{ to }600\text{ nm}$  emphasizes the role of local and regional anthropogenic sources for that size range. A maximum persistence was found for particle concentrations at  $600\text{ nm}$ , which are the most representative for long-range transported aerosol. Coarse particles  $>2\text{ }\mu\text{m}$  were characterised by a mixture of a persistent and a periodic behaviour.

When heating the ambient aerosol to  $300^{\circ}\text{C}$  in a thermodenuder (TD), about 69% of the particulate volume ( $<800\text{ nm}$ ) vanished, while particle number ( $>6\text{ nm}$ ) remained constant within the measurement accuracy. The summation method was applied to derive diameter shrinking factors (SF) due to the volatilisation step as a function of particle size. Particles between  $60\text{ and }200\text{ nm}$  shrank, on average, to  $0.55\text{--}0.70$  of their original diameter. Towards smaller particles ( $30\text{ nm}$ ), the non-volatile fraction decreased, but increased towards bigger particles ( $300\text{ nm}$ ).

The diurnal cycle of SF showed a relative maximum for  $80\text{ nm}$  during the morning peak traffic hours (08:00) while for  $30\text{ nm}$  a relative minimum occurred. This emphasizes the presence of soot in traffic-derived  $80\text{ nm}$  particles but also its absence in particulate traffic emissions  $<30\text{ nm}$ . Correlations between the non-volatile particle volume and ( $<800\text{ nm}$ ) an optically derived  $\text{PM}_{2.5}$  soot concentration yielded measures of determination ( $R^2$ ) between  $0.76$  and  $0.85$ , suggesting a strong association between the non-volatile particle residues and soot.

The meteorological analysis involved a separation of the data set according to local wind direction, the mixed layer height, and back trajectories. The prime result was that the height of the planetary boundary layer played the most important role on the

## Size distributions before and after volatilisation

W. Birmili et al.

Title Page

Abstract

Introduction

Conclusions

References

Tables

Figures

◀

▶

◀

▶

Back

Close

Full Screen / Esc

Printer-friendly Version

Interactive Discussion



---

**Size distributions  
before and after  
volatilisation**W. Birmili et al.

---

[Title Page](#)[Abstract](#)[Introduction](#)[Conclusions](#)[References](#)[Tables](#)[Figures](#)[◀](#)[▶](#)[◀](#)[▶](#)[Back](#)[Close](#)[Full Screen / Esc](#)[Printer-friendly Version](#)[Interactive Discussion](#)

particle number concentrations in the urban atmosphere of Augsburg. The highest particle number concentrations >30 nm were associated with the most stable inversion situations, and, slightly surprisingly, not necessarily with air masses from the continental source regions of Eastern Europe. The importance of the mixing layer height found here confirms earlier studies of surface-measured particle mass concentrations in urban areas (e.g. Schäfer et al., 2006).

It is a main conclusion that the particle size distribution in an urban area such as Augsburg is shaped by a combination of relatively few effects. The vertical stability of the atmosphere, particularly, proved to be a very influential factor, more important for instance than the local or large-scale wind direction. Our results are worth considering when using the particle data in future epidemiological studies, or in particle exposure assessments.

## Appendix A

### Detailed time history

Figure 15 shows the detailed time histories of ambient temperature and the number concentration of 600 nm-particles in Augsburg for the two winters 2004/2005 and 2005/2006, respectively. The seven marked episodes with high particle concentrations are discussed in Sect. 3.1.2.

*Acknowledgements.* We acknowledge Dr Hans Kaufmann (FH Augsburg) for providing the wind measurements at the roof-top station. Back trajectories were calculated on the NOAA ARL Ready Website using the HYSPLIT (HYbrid Single-Particle Lagrangian Integrated Trajectory) Model (Draxler, R. R. and Hess, G. D., 2003, NOAA Air Resources Laboratory, Silver Spring, MD, USA). Radiosoundings at Oberschleiheim were made by the German Weather Service DWD and accessed through the University of Wyoming website (<http://weather.uwyo.edu/upperair/>). We thank Christa Engler for characterising the particle transmission of the thermodenunder. The data evaluation for this paper was supported by the European Integrated

## References

- Aalto, P., Hämeri, K., Paatero, P., et al.: Aerosol particle number concentration measurements in five European cities using TSI-3022 Condensation Particle Counter over three-year period during health effects of air pollution on susceptible subpopulations, *J. Air Waste Manage. Assoc.*, 55, 1064–1076, 2005. 9174, 9181, 9183
- An, W., Pathak, R., Lee, B., et al.: Aerosol volatility measurement using an improved thermodenuder: Application to secondary organic aerosol, *J. Aerosol Sci.*, 38, 305–314, 2007. 9174
- Birmili, W., Stratmann, F., and Wiedensohler, A.: Design of a DMA-based size spectrometer for a large particle size range and stable operation, *J. Aerosol Sci.*, 30, 549–553, 1999. 9176
- Birmili, W., Wiedensohler, A., Heintzenberg, J., and Lehmann, K.: Atmospheric particle number size distribution in Central Europe: Statistical relations to air masses and meteorology, *J. Geophys. Res.*, 106(D23), 32005–32018, 2001. 9192
- Birmili, W., Schwirn, K., Nowak, A., et al.: Hygroscopic growth of atmospheric particle number size distributions in the Finnish boreal forest region, *Bor. Env. Res.*, in press, 2009. 9179
- Burtscher, H., Baltensperger, U., Bukowiecki, N., et al.: Separation of volatile and non-volatile aerosol fractions by thermodesorption: instrumental development and applications, *J. Aerosol Sci.*, 32, 427–442, 2001. 9174
- Charron, A. and Harrison, R. M.: Primary particle formation from vehicle emissions during exhaust dilution in the roadside atmosphere, *Atmos. Env.*, 37, 4109–4119, 2003. 9174
- Costabile, F., Birmili, W., Klose, S., Tuch, T., Wehner, B., Wiedensohler, A., Franck, U., König, K., and Sonntag, A.: Spatio-temporal variability and principal components of the particle number size distribution in an urban atmosphere, *Atmos. Chem. Phys. Discuss.*, 8, 18155–18217, 2008, <http://www.atmos-chem-phys-discuss.net/8/18155/2008/>. 9174, 9185
- Cyrys, J., Stölzel, M., Kreyling, W. G. et al.: Sources and elemental composition of ambient particles in Erfurt, Germany, *Sci. Total Environ.*, 305, 143–156, 2003. 9184

## Size distributions before and after volatilisation

W. Birmili et al.

Title Page

Abstract

Introduction

Conclusions

References

Tables

Figures

◀

▶

◀

▶

Back

Close

Full Screen / Esc

Printer-friendly Version

Interactive Discussion



- Cyrys, J., Pitz, M., Heinrich, J., et al.: Spatial and temporal variation of particle number concentration in Augsburg, Germany, *Sci. Total Environ.*, 401, 168–175, 2008. 9176
- Draxler, R. and Hess, G.: Description of the HYSPLIT4 modeling system, NOAA Technical Memorandum, ERL, ARL-224, 2004. 9180
- 5 Ebel, S., Cyrys, J., Brauer, S., et al.: Air Quality in Postunification Erfurt, East Germany: Associating changes in pollutant concentrations with changes in emissions, *Environ. Health Persp.*, 109, 325–333, 2001. 9174
- EC: Council Directive 1999/30/EC, of 22 April 1999: Limit values for sulphur dioxide, nitrogen dioxide and oxides of nitrogen, particulate matter and lead in ambient air (The First Daughter Directive), 1999. 9173
- 10 Ehn, M., Petäjä, T., Birmili, W., Junninen, H., Aalto, P., and Kulmala, M.: Non-volatile residuals of newly formed atmospheric particles in the boreal forest, *Atmos. Chem. Phys.*, 7, 677–684, 2007, <http://www.atmos-chem-phys.net/7/677/2007/>. 9175, 9186
- 15 Engler, C., Rose, D., Wehner, B., Wiedensohler, A., Brüggemann, E., Gnauk, T., Spindler, G., Tuch, T., and Birmili, W.: Size distributions of non-volatile particle residuals ( $D_p < 800$  nm) at a rural site in Germany and relation to air mass origin, *Atmos. Chem. Phys.*, 7, 5785–5802, 2007, <http://www.atmos-chem-phys.net/7/5785/2007/>. 9179, 9180, 9187
- 20 Fierz, M., Vernooij, M., and Burtscher, H.: An improved low-flow thermodenuder, *J. Aerosol Sci.*, 38, 1163–1168, 2007. 9174
- Hasegawa, S., Hirabayashi, M., Kobayashi, S., et al.: Size distribution and characterization of ultrafine particles in roadside atmosphere, *J. Environ. Sci. Heal. A.*, 39, 2671–2690, 2004. 9175
- 25 HEI: Understanding the health effects of components of the particulate matter mix: progress and next steps, Tech. Rep. 4, Health Effects Institute, Boston, MA, 2002. 9173
- Hitchins, J., Morawska, L., Wolff, R., and Gilbert, D.: Concentrations of submicrometre particles from vehicle emissions near a major road, *Atmos. Env.*, 34, 51–59, 2000. 9174
- Holle, R., Happich, M., Löwel, H., and Wichmann, H.: KORA – A Research platform for population based health research, *Gesundheitswesen*, 67, S19–S25, 2005. 9175
- 30 Holzworth, C. G.: Estimates of mean maximum mixing depths in the contiguous United States, *Mon. Weather Rev.*, 92, 235–242, 1964. 9180
- Huffman, J., Ziemann, P., Jayne, J., Worsnop, D., and Jimenez, J.: Development and character-

---

**Size distributions  
before and after  
volatilisation**W. Birmili et al.

---

Title Page

Abstract

Introduction

Conclusions

References

Tables

Figures

◀

▶

◀

▶

Back

Close

Full Screen / Esc

Printer-friendly Version

Interactive Discussion



**Size distributions  
before and after  
volatilisation**

W. Birmili et al.

Title Page

Abstract

Introduction

Conclusions

References

Tables

Figures

◀

▶

◀

▶

Back

Close

Full Screen / Esc

Printer-friendly Version

Interactive Discussion



ization of a fast-stepping/scanning thermodenuder for chemically-resolved aerosol volatility measurements, *Aerosol Sci. Technol.*, 42, 395–407, 2008. 9174

Hussein, T., Puustinen, A., Aalto, P. P., Mäkelä, J. M., Hämeri, K., and Kulmala, M.: Urban aerosol number size distributions, *Atmos. Chem. Phys.*, 4, 391–411, 2004,

<http://www.atmos-chem-phys.net/4/391/2004/>. 9174, 9183

Imhof, D., Weingartner, E., Ordóñez, C., et al.: Real-world emission factors of fine and ultrafine aerosol particles for different traffic situations in Switzerland, *Env. Sci. Technol.*, 39, 8341–8350, 2005. 9174

Kalberer, M., Paulsen, D., Sax, M., et al.: Identification of polymers as major components of atmospheric organic aerosols, *Science*, 303, 1659–1662, 2004. 9187

Ketzel, M., Wahlin, P., Berkowicz, R., and Palmgren, F.: Particle and trace gas emission factors under urban driving conditions in Copenhagen based on street and roof-level observations, *Atmos. Env.*, 37, 2735–2749, 2003. 9174

Ketzel, M., Wählín, P., Kristensson, A., Swietlicki, E., Berkowicz, R., Nielsen, O. J., and Palmgren, F.: Particle size distribution and particle mass measurements at urban, near-city and rural level in the Copenhagen area and Southern Sweden, *Atmos. Chem. Phys.*, 4, 281–292, 2004,

<http://www.atmos-chem-phys.net/4/281/2004/>. 9174, 9182

Kittelson, D., Watts, W., and Johnson, J.: On-road and laboratory evaluation of combustion aerosols – Part 1: Summary of diesel engine results, *J. Aerosol Sci.*, 37, 913–930, 2006. 9186

Keyling, W. and Scheuch, G.: Clearance of particles deposited in the lungs, in *Particle-Lung Interactions*, edited by P. Gehr and J. Heyder, 323–376, Marcel Dekker, New York, 2000. 9173

Keyling, W., Tuch, T., Peters, A. et al.: Diverging long-term trends in ambient urban particle mass and number concentrations associated with emission changes caused by the German unification, *Atmos. Env.*, 37, 3841–3848, 2003. 9174

Kukkonen, J., Pohjola, M., Sokhi, R. et al.: Analysis and evaluation of local scale PM10 air pollution episodes in four European cities: Helsinki, London, Milan and Oslo, *Atmos. Env.*, 39, 2759–2773, 2005. 9190

Kulmala, M., Vehkamäki, H., Petäjä, T., et al.: Formation and growth rates of ultrafine atmospheric particles: A review of observations, *J. Aerosol Sci.*, 35, 143–176, 2004. 9174

Möller, W., Felten, K., Sommerer, K., et al.: Deposition, retention, and translocation of ultrafine

particles from the central airways and lung periphery, *Am. J. Resp. Crit. Care Med.*, 177, 426–432, 2008. 9173

Ntziachristos, L., Mamakos, A., Samaras, Z., et al.: Overview of the European Particulates project on the characterization of exhaust particulate emissions from road vehicles: Results for light-duty vehicles, *SAE transactions*, 113, 1354–1373, 2004. 9174, 9186

Oberdörster, G., Oberdörster, G., and Oberdörster, G.: Nanotoxicology: an emerging discipline evolving from studies of ultrafine particles, *Environ. Health Persp.*, 113, 823–839, 2005. 9173

Peters, A., von Klot, S., Heier, M., et al.: Particulate air pollution and nonfatal cardiac events. Part I. air pollution, personal activities, and onset of myocardial infarction in a case-crossover study, *HEI Research Report*, 124, 1–82, 2005. 9175

Philippin, S., Wiedensohler, A., and Stratmann, F.: Measurements of non-volatile fractions of pollution aerosols with an eight-tube volatility tandem differential mobility analyzer (VTDMA-8), *J. Aerosol Sci.*, 35, 185–203, 2004. 9175

Pitz, M., Schmid, O., Heinrich, J., et al.: Seasonal and diurnal variation of PM<sub>2.5</sub> apparent particle density in urban air in Augsburg, Germany, *Env. Sci. Technol.*, 42, 5087–5093, 2008a. 9176

Pitz, M., Birmili, W., Schmid, O., Peters, A., and Cyrys, J.: Quality assurance of aerosol particle size distribution measurements at an urban air pollution monitoring station in Augsburg, Germany, *J. Env. Mon.*, 10, 1017–1024, 2008b. 9178, 9189

Pope, C. and Dockery, D.: Health effects of fine particulate air pollution: lines that connect, *J. Air Waste Manage. Assoc.*, 56, 709–742, 2006. 9173

Rose, D., Wehner, B., Ketzel, M. et al.: Atmospheric number size distributions of soot particles and estimation of emission factors, *Atmos. Chem. Phys.*, 6, 1021–1031, 2006, <http://www.atmos-chem-phys.net/6/1021/2006/>. 9175, 9186

Rosenbohm, E., Vogt, R., Scheer, V., et al.: Particulate size distributions and mass measured at a motorway during the BAB II campaign, *Atmos. Env.*, 39, 5696–5709, 2005. 9174

Ruuskanen, J., Tuch, T., and ten Brink, H.: Concentrations of ultrafine, fine and PM<sub>2.5</sub> particles in three European cities, *Atmos. Env.*, 35, 3729–3738, 2001. 9181

Sakurai, H., Park, K., McMurry, P., et al.: Size-dependent mixing characteristics of volatile and nonvolatile components in diesel exhaust aerosols, *Env. Sci. Technol.*, 37, 5487–5495, 2003. 9174, 9186, 9188

Schäfer, K., Emeis, S., Hoffmann, H., and Jahn, C.: Influence of mixing layer height upon air pollution in urban and sub-urban areas, *Meteorolog. Z.*, 15, 647–658, 2006. 9190, 9194

**Size distributions  
before and after  
volatilisation**

W. Birmili et al.

Title Page

Abstract

Introduction

Conclusions

References

Tables

Figures

◀

▶

◀

▶

Back

Close

Full Screen / Esc

Printer-friendly Version

Interactive Discussion



- Schmid, O., Eimer, B., Hagen, D., et al.: Investigation of volatility methods for measuring aqueous sulfuric acid on mixed aerosols, *Aerosol Sci. Technol.*, 36, 877–889, 2002. 9174
- Schwarze, P., Ovrevik, J., and Lag, M.: Particulate matter properties and health effects: Consistency of epidemiological and toxicological studies, *Hum. Exp. Toxicol.*, 25, 559–579, 2006. 9173
- Sheridan, P., Arnott, W., Ogren, J., et al.: The Reno Aerosol Optics Study: An evaluation of aerosol absorption measurement methods, *Aerosol Sci. Technol.*, 39, 1–16, 2005. 9178
- Sioutas, C., Delfino, R., and Singh, M.: Exposure assessment for atmospheric ultrafine particles (UFPs) and implications in epidemiologic research, *Environ. Health Persp.*, 113, 947–955, 2005. 9173
- Stanier, C., Khlystov, A., and Pandis, S.: Ambient aerosol size distributions and number concentrations measured during the Pittsburgh air quality study, *Atmos. Env.*, 38, 3275–3284, 2004. 9182
- Stull, R.: An introduction to boundary layer meteorology, Reidel Publishing, Dordrecht, 1988. 9180
- Thorpe, A. and Harrison, R. M.: Sources and properties of non-exhaust particulate matter from road traffic: A review, *Sci. Tot. Env.*, 400, 270–282, 2008. 9183
- Tunved, P., Hansson, H.-C., Kulmala, M., Aalto, P., Viisanen, Y., Karlsson, H., Kristensson, A., Swietlicki, E., Dal Maso, M., Strm, J., and Komppula, M.: One year boundary layer aerosol size distribution data from five nordic background stations, *Atmos. Chem. Phys.*, 3, 2183–2205, 2003, <http://www.atmos-chem-phys.net/3/2183/2003/>. 9192
- van Dingenen, R., Raes, F., Puteaud, J.-P., et al.: A European aerosol phenomenology-1: Physical characteristics of particulate matter at kerbside, urban, rural and background sites in Europe, *Atmos. Env.*, 38, 2561–2577, 2004. 9174
- Vester, B., Ebert, M., Barnert, E., et al.: Composition and mixing state of the urban background aerosol in the Rhein-Main area (Germany), *Atmos. Env.*, 41, 6102–6115, 2007. 9186, 9187
- Voigtländer, J., Tuch, T., Birmili, W., and Wiedensohler, A.: Correlation between traffic density and particle size distribution in a street canyon and the dependence on wind direction, *Atmos. Chem. Phys.*, 6, 4275–4286, 2006, <http://www.atmos-chem-phys.net/6/4275/2006/>. 9174
- von Klot, S., Peters, A., Aalto, P. et al.: Ambient air pollution is associated with increased risk of hospital cardiac readmissions of myocardial infarction survivors in five European cities.

---

**Size distributions  
before and after  
volatilisation**W. Birmili et al.

---

Title Page

Abstract

Introduction

Conclusions

References

Tables

Figures

◀

▶

◀

▶

Back

Close

Full Screen / Esc

Printer-friendly Version

Interactive Discussion



**Size distributions  
before and after  
volatilisation**

W. Birmili et al.

[Title Page](#)[Abstract](#)[Introduction](#)[Conclusions](#)[References](#)[Tables](#)[Figures](#)[◀](#)[▶](#)[◀](#)[▶](#)[Back](#)[Close](#)[Full Screen / Esc](#)[Printer-friendly Version](#)[Interactive Discussion](#)

Report of the Health Effects of Particles on Susceptible Subpopulations (HEAPSS) Study Group, *Circulation*, 112, 3073–3079, 2005. 9173, 9175

Wehner, B., Birmili, W., Gnauk, T., and Wiedensohler, A.: Particle number size distributions in a street canyon and their transformation into the urban background: Measurements and a simple model study, *Atmos. Env.*, 36, 2215–2223, 2002a. 9174

Wehner, B., Philippin, S., Wiedensohler, A., and Haudek, A.: Design and calibration of an improved thermodenuder to study the volatility fraction of aerosol particles, *J. Aerosol Sci.*, 33, 1087–1093, 2002b. 9174, 9176

Wehner, B. and Wiedensohler, A.: Long term measurements of submicrometer urban aerosols: Statistical analysis for correlations with meteorological conditions and trace gases, *Atmos. Chem. Phys.*, 3, 867–879, 2003, <http://www.atmos-chem-phys.net/3/867/2003/>. 9174, 9182, 9183, 9184

Wehner, B., Petäjä, T., Boy, M., et al.: The contribution of sulfuric acid and non-volatile compounds on the growth of freshly formed atmospheric aerosols, *Geophys. Res. Lett.*, 32, L17810, doi:10.1029/2005GL023827, 2005. 9175, 9186

Wehner, B., Birmili, W., Ditas, F., Wu, Z., Hu, M., Liu, X., Mao, J., Sugimoto, N., and Wiedensohler, A.: Relationships between submicrometer particulate air pollution and air mass history in Beijing, China, 2004–2006, *Atmos. Chem. Phys.*, 8, 6155–6168, 2008, <http://www.atmos-chem-phys.net/8/6155/2008/>. 9182

WHO: Health Effects of Air Pollution Results from the WHO Project *Systematic Review of Health Aspects of Air Pollution in Europe*, Tech. Rep. E83080, World Health Organisation, Geneva, 2004. 9173

WHO: Health risks of particulate matter from long-range transboundary air pollution, joint WHO/Convention Task Force on the Health Aspects of Air Pollution, WHOLIS E88189, World Health Organisation, Regional Office for Europe, Bonn, 2006. 9173

Wichmann, H.-E. and Peters, A.: Epidemiological evidence of the effects of ultrafine particle exposure, *Phil. Trans. R. Soc. Lond.*, 358, 2751–2769, 2000. 9173

Wichmann, H.-E., Cyrus, J., Stölzel, M. et al.: Sources and elemental composition of ambient particles in Erfurt, Germany, Ecomed Verlag, Landsberg am Lech, 2002. 9183

Woo, K. S., Chen, D.-R., Pui, D. Y. H., and McMurry, P.H.: Measurements of Atlanta aerosol size distribution: Observation of ultrafine particle events, *Aerosol Sci. Technol.*, 34(1), 75–87, 2001. 9182

Zhu, Y., Hinds, W., Shen, S., and Sioutas, C.: Seasonal and spatial trends in fine particulate matter – seasonal trends of concentration and size distribution of ultrafine particles near major highways in Los Angeles, *Aerosol Sci. Technol.*, 38, 5–13, 2004. 9174

ACPD

9, 9171–9220, 2009

---

**Size distributions  
before and after  
volatilisation**

W. Birmili et al.

---

Title Page

Abstract

Introduction

Conclusions

References

Tables

Figures

⏪

⏩

◀

▶

Back

Close

Full Screen / Esc

Printer-friendly Version

Interactive Discussion



## Size distributions before and after volatilisation

W. Birmili et al.

**Table 1.** Particle number concentrations in Augsburg for specific particle size intervals.  $\mu$  indicates the arithmetic mean,  $\sigma$  the standard deviation,  $\sigma_\mu$  the standard deviation of the mean, and  $p_k$  the  $k$ th percentile of the concentration in the corresponding size interval.

$D_p$ range	$\mu$	$\sigma_\mu$	$\sigma$	$p_1$	$p_5$	$p_{25}$	$p_{50}$	$p_{75}$	$p_{95}$	$p_{99}$
3–10 nm	790	19	1300	74	140	310	530	870	1900	6300
10–30 nm	3700	46	3000	530	850	1700	2900	4700	9300	15000
30–300 nm	7600	96	6300	1300	2100	3800	5900	9400	19000	30000
300–800 nm	150	3	170	930	17	4700	100	200	430	850
800–2000 nm	2	0.04	3	0.12	0.27	0.65	1	2	7	1500
2000–10 000 nm	0.16	0.01	0.13	0.01	0.03	0.07	0.12	0.20	0.39	0.65

[Title Page](#)
[Abstract](#)
[Introduction](#)
[Conclusions](#)
[References](#)
[Tables](#)
[Figures](#)
[Back](#)
[Close](#)
[Full Screen / Esc](#)
[Printer-friendly Version](#)
[Interactive Discussion](#)


**Table 2.** Mean characteristics of the 13 back trajectory clusters. Season index (SI) reflects occurrence in winter (−1) or summer (+1). WD: wind direction, WS: wind speed, MLH: mixed layer height,  $N_{[5-800]}$ : total particle number between 5 and 800 nm,  $N_{nv[30-800]}$ : particle number downstream of the thermodenuder (300°C) between 30 and 800 nm.

No.	WD	Frequency days	%	$N_{[5-800]}$ $\text{cm}^{-3}$	$N_{nv[30-800]}$ $\text{cm}^{-3}$	SI	MLH m	$WS_{\text{traj}}$ $\text{m s}^{-1}$	$WD_{\text{traj}}$	$WS_{\text{local}}$ $\text{m s}^{-1}$	$WD_{\text{local}}$
1	W	28	5	9100	2100	−0.4	1100	1.9	247°	3.8	214°(±20)
2	SW	43	7	8000	1900	−0.1	800	2.2	254°	3.5	220°(±10)
3	NW	80	14	7300	2200	0.2	730	1.7	268°	3.2	236°(±10)
4	SW	25	4	17 000	6400	−0.4	450	0.8	230°	1.5	141°(±30)
5	S	78	13	8000	2600	0.1	540	1.3	259°	2.7	207°(±20)
6	W	75	13	8500	3100	0.5	720	0.6	0°	2.0	162°(±50)
7	O	27	5	10 500	3900	0.2	650	0.3	121°	2.0	120°(±20)
8	O	24	4	17 000	6500	−0.6	430	0.4	152°	1.8	113°(±30)
9	NO	33	6	13 500	3700	−0.6	400	0.3	75°	2.3	119°(±50)
10	NW	83	14	13 000	3900	−0.2	560	0.6	291°	2.4	184°(±80)
11	NO	42	7	13 000	3600	0.1	730	0.9	45°	2.8	134°(±80)
12	N	13	2	19 000	6200	−0.6	760	0.8	226°	1.9	173°(±30)
13	N	43	7	10 500	2600	0.1	1000	0.9	288°	3.0	207°(±20)

## Size distributions before and after volatilisation

W. Birmili et al.

Title Page

Abstract

Introduction

Conclusions

References

Tables

Figures

◀

▶

◀

▶

Back

Close

Full Screen / Esc

Printer-friendly Version

Interactive Discussion

Size distributions  
before and after  
volatilisation

W. Birmili et al.

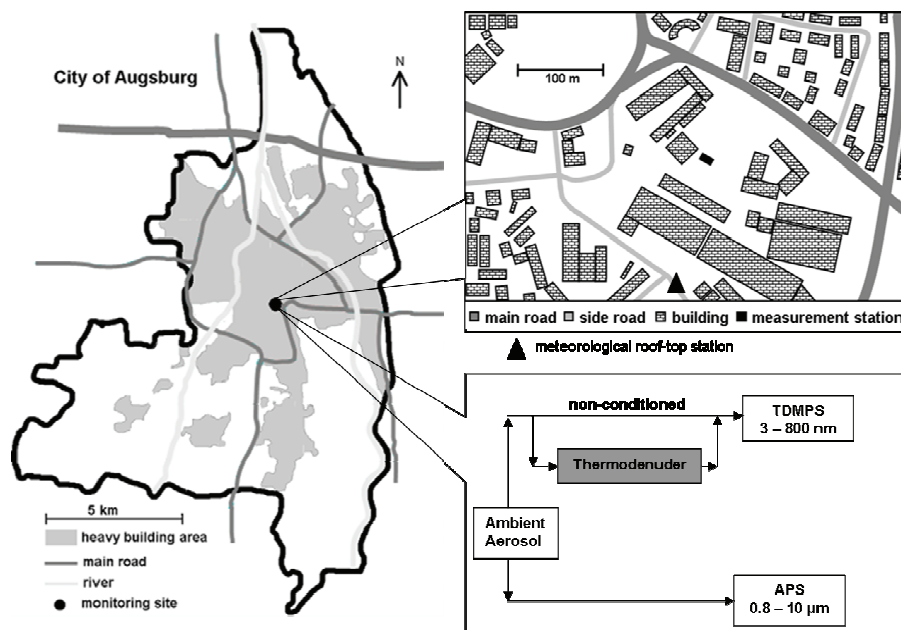


**Fig. 1.** Regional map of Augsburg, Germany, including the detailed surroundings of the HMGU monitoring station. The lower inset illustrates the concurrent measurement of TDMPS and APS size distributions with the option of using a thermodenuder upstream the TDMPS.

[Title Page](#)[Abstract](#)[Introduction](#)[Conclusions](#)[References](#)[Tables](#)[Figures](#)[◀](#)[▶](#)[◀](#)[▶](#)[Back](#)[Close](#)[Full Screen / Esc](#)[Printer-friendly Version](#)[Interactive Discussion](#)

**Size distributions  
before and after  
volatilisation**

W. Birmili et al.

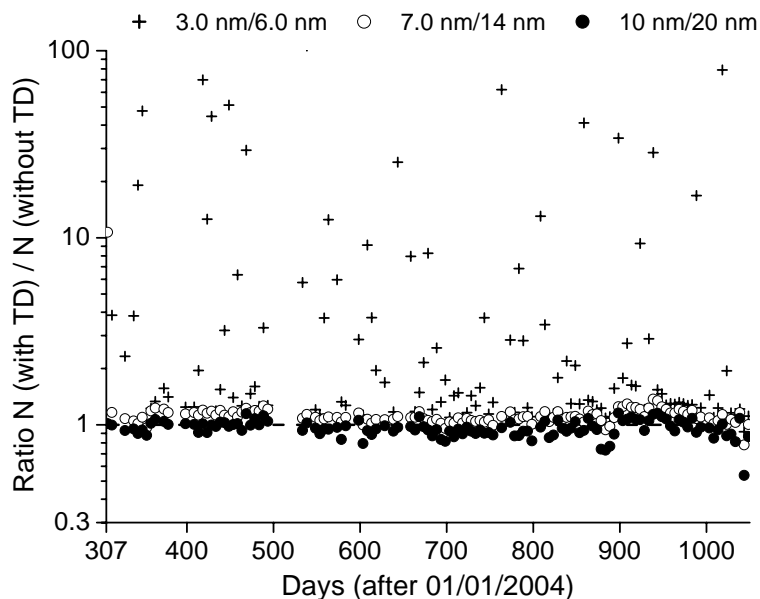


**Fig. 2.** Ratio between the total particle number concentrations upstream and downstream the thermodenuder. The labels indicate the pairs of lower threshold diameters that were applied to the non-conditioned and conditioned size distributions, respectively, before computing the integral number concentration. When ignoring size channels below 7 nm (i.e. those affected by artificial nucleation inside the thermodenuder, the particle number balance across the thermodenuder becomes approximately unity. Time is coded in days after 01/01/2004. Plotted is every fifth daily average value of the measurement campaign.

[Title Page](#)[Abstract](#)[Introduction](#)[Conclusions](#)[References](#)[Tables](#)[Figures](#)[◀](#)[▶](#)[◀](#)[▶](#)[Back](#)[Close](#)[Full Screen / Esc](#)[Printer-friendly Version](#)[Interactive Discussion](#)

Size distributions  
before and after  
volatilisation

W. Birmili et al.

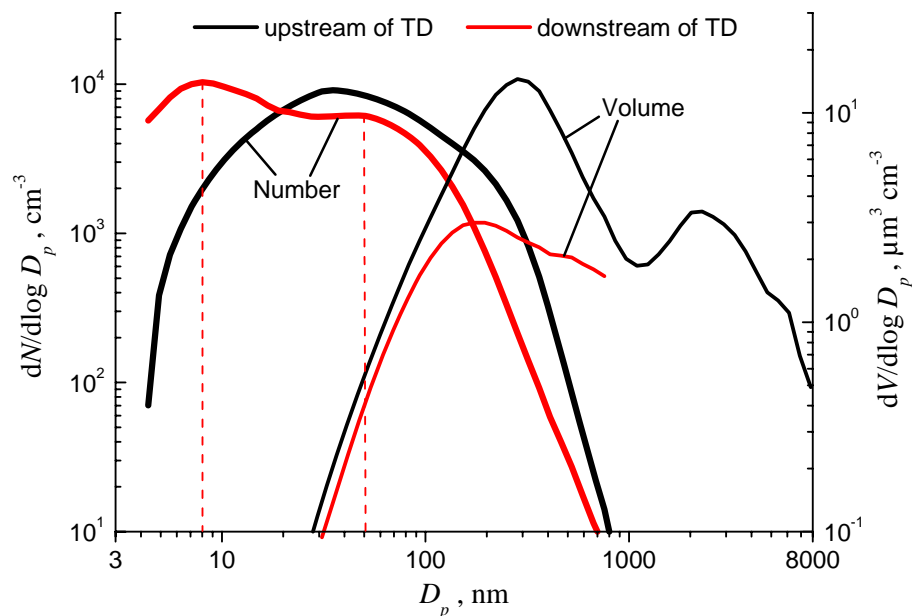


**Fig. 3.** Median number and volume size distributions of ambient (TDMPS/APS) and non-volatile (TDMPS with TD) particle concentrations in Augsburg between 11/2004 and 11/2006. Volume size distributions were calculated assuming spherical particles. Dashed lines mark the location of the two particles modes in the non-volatile distribution.

[Title Page](#)[Abstract](#)[Introduction](#)[Conclusions](#)[References](#)[Tables](#)[Figures](#)[◀](#)[▶](#)[◀](#)[▶](#)[Back](#)[Close](#)[Full Screen / Esc](#)[Printer-friendly Version](#)[Interactive Discussion](#)

Size distributions  
before and after  
volatilisation

W. Birmili et al.

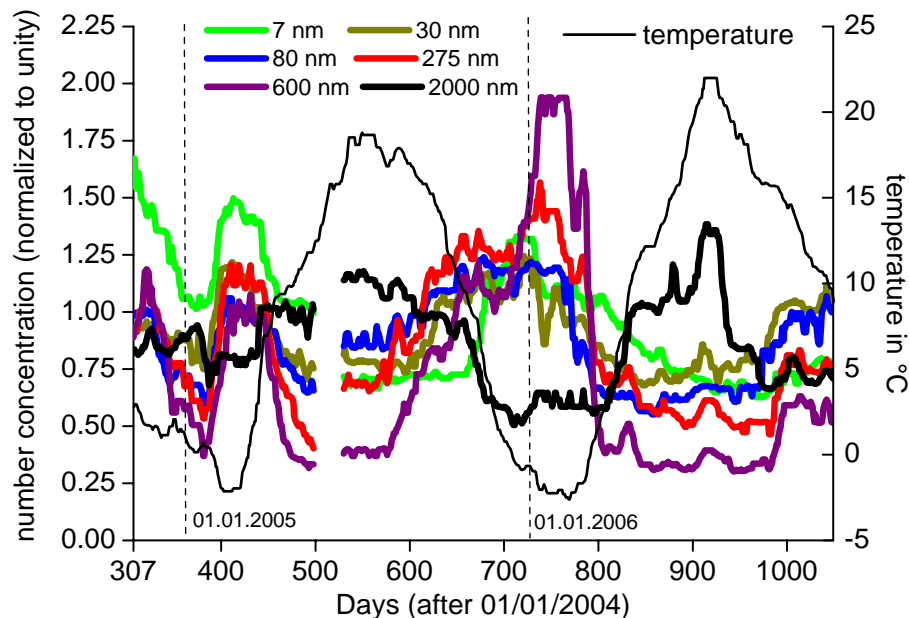


**Fig. 4.** Time series of particle number concentration (30-day running median values) over the entire two-year period. Shown are the particle concentrations at discrete particle diameters, each normalised to an average of unity. Time is coded in days after 01/01/2004. The thin line indicates ambient temperature (30-day running median).

[Title Page](#)[Abstract](#)[Introduction](#)[Conclusions](#)[References](#)[Tables](#)[Figures](#)[◀](#)[▶](#)[◀](#)[▶](#)[Back](#)[Close](#)[Full Screen / Esc](#)[Printer-friendly Version](#)[Interactive Discussion](#)

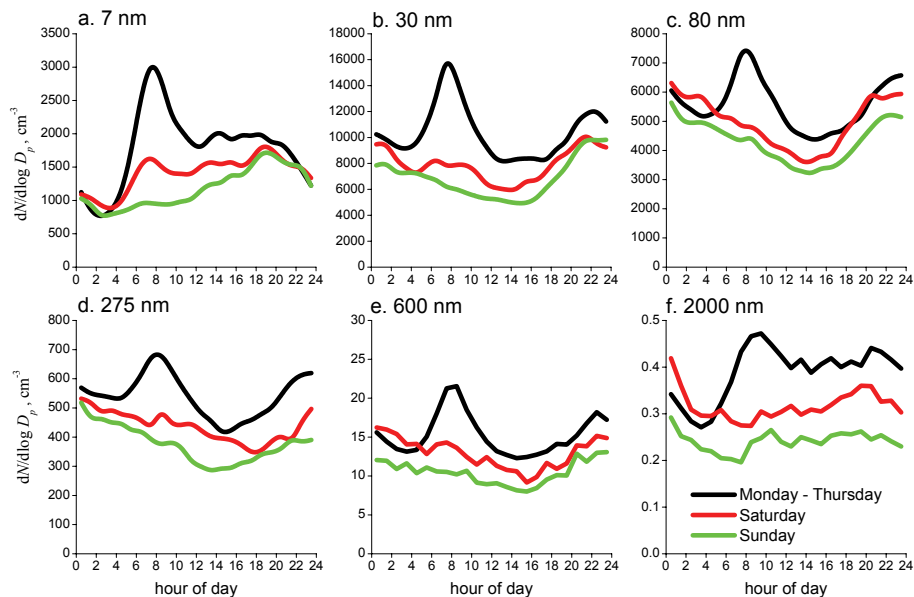


**Fig. 5.** Average diurnal cycle of particle number concentration at **(a)** 7 nm, **(b)** 30 nm, **(c)** 80 nm, **(d)** 275 nm, **(e)** 600 nm and **(f)** 2000 nm. The data cover the entire measurement campaigning and are keyed after different periods of the week.

## Size distributions before and after volatilisation

W. Birmili et al.

Title Page

Abstract

Introduction

Conclusions

References

Tables

Figures

◀

▶

◀

▶

Back

Close

Full Screen / Esc

Printer-friendly Version

Interactive Discussion



**Size distributions  
before and after  
volatilisation**

W. Birmili et al.

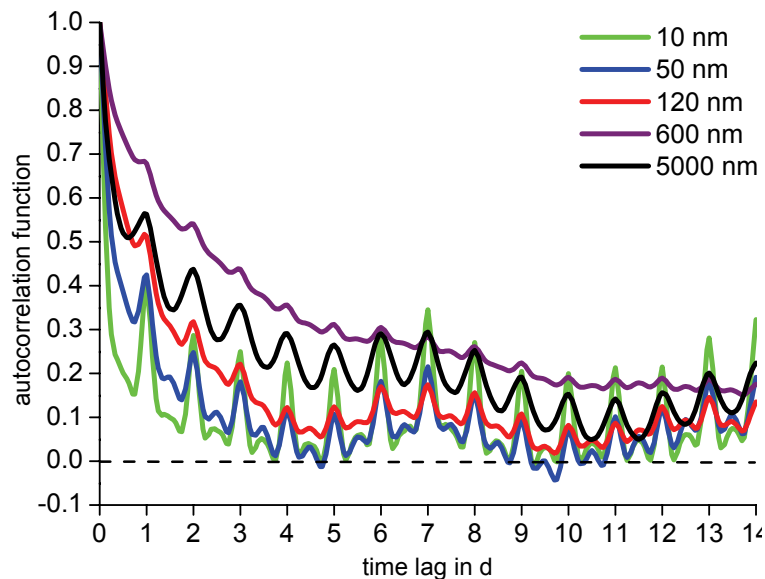


**Fig. 6.** Auto-correlation function of particle number concentration at selected particle diameters.

[Title Page](#)[Abstract](#)[Introduction](#)[Conclusions](#)[References](#)[Tables](#)[Figures](#)[◀](#)[▶](#)[◀](#)[▶](#)[Back](#)[Close](#)[Full Screen / Esc](#)[Printer-friendly Version](#)[Interactive Discussion](#)

Size distributions  
before and after  
volatilisation

W. Birmili et al.

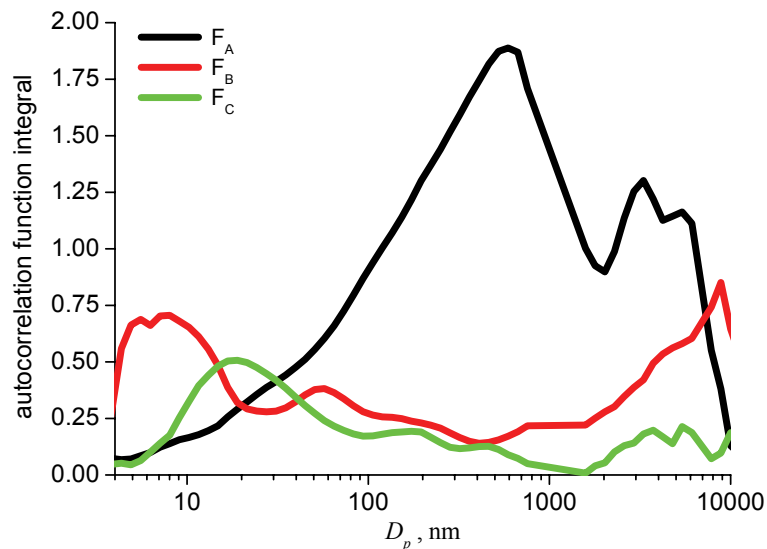


**Fig. 7.** Integrals of the three auto-correlation function components ( $0 < t < 14$  d) as a function of particle diameter  $D_p$ . Here,  $F_A$  is the persistent (long-lasting) component,  $F_B$  the daily periodical component and  $F_C$  the weekly periodical component.

[Title Page](#)[Abstract](#)[Introduction](#)[Conclusions](#)[References](#)[Tables](#)[Figures](#)[◀](#)[▶](#)[◀](#)[▶](#)[Back](#)[Close](#)[Full Screen / Esc](#)[Printer-friendly Version](#)[Interactive Discussion](#)

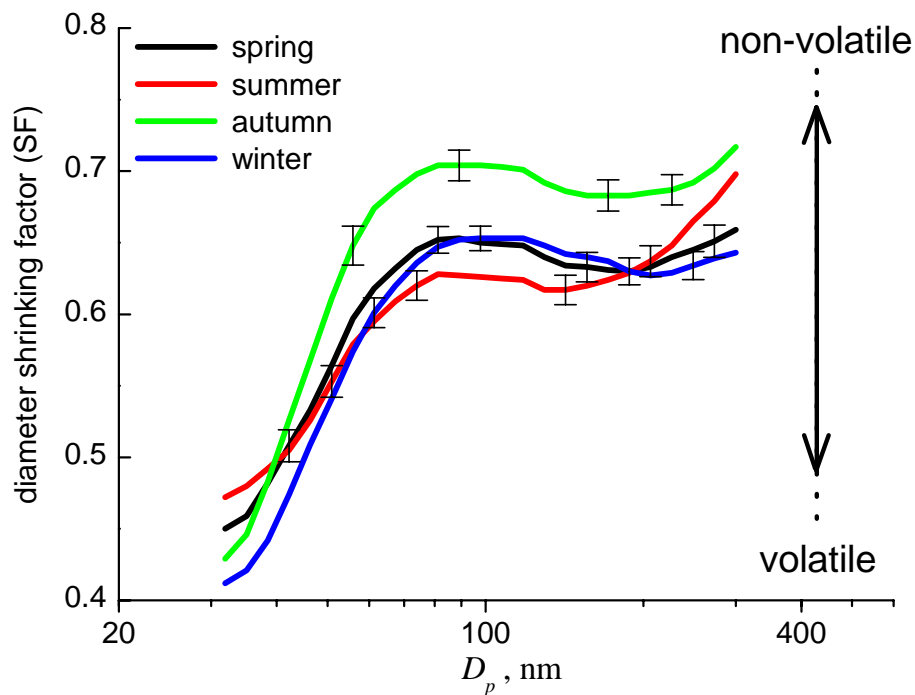


**Fig. 8.** Particle diameter shrinking factor (SF) due to thermodesorption at 300°C. The data cover the morning traffic peak hours (06:00–09:00 CET) and are keyed after season. Whiskers represent plus/minus one sigma of the mean.

## Size distributions before and after volatilisation

W. Birmili et al.

Title Page

Abstract

Introduction

Conclusions

References

Tables

Figures

◀

▶

◀

▶

Back

Close

Full Screen / Esc

Printer-friendly Version

Interactive Discussion



Size distributions  
before and after  
volatilisation

W. Birmili et al.

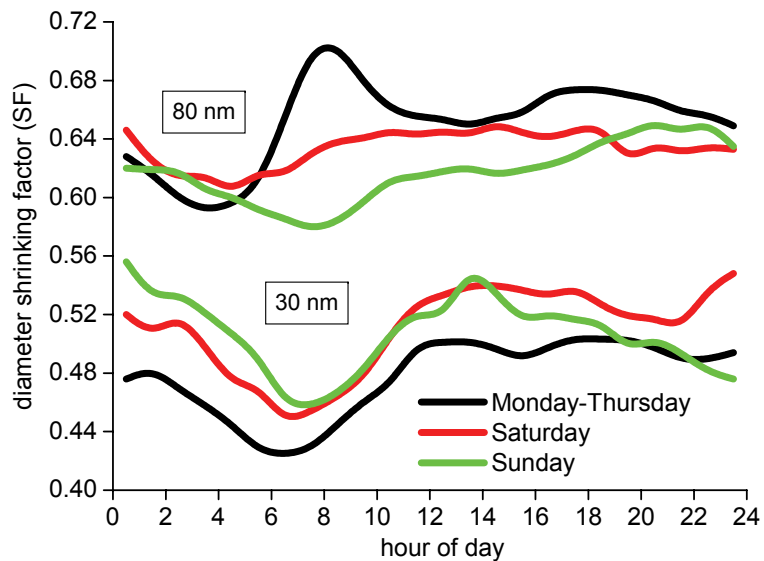


**Fig. 9.** Average diurnal cycle of the diameter shrinking factor (SF) of 30 nm and 80 nm particles. The data are also distinguished between weekdays and weekends.

[Title Page](#)[Abstract](#)[Introduction](#)[Conclusions](#)[References](#)[Tables](#)[Figures](#)[◀](#)[▶](#)[◀](#)[▶](#)[Back](#)[Close](#)[Full Screen / Esc](#)[Printer-friendly Version](#)[Interactive Discussion](#)

Size distributions  
before and after  
volatilisation

W. Birmili et al.

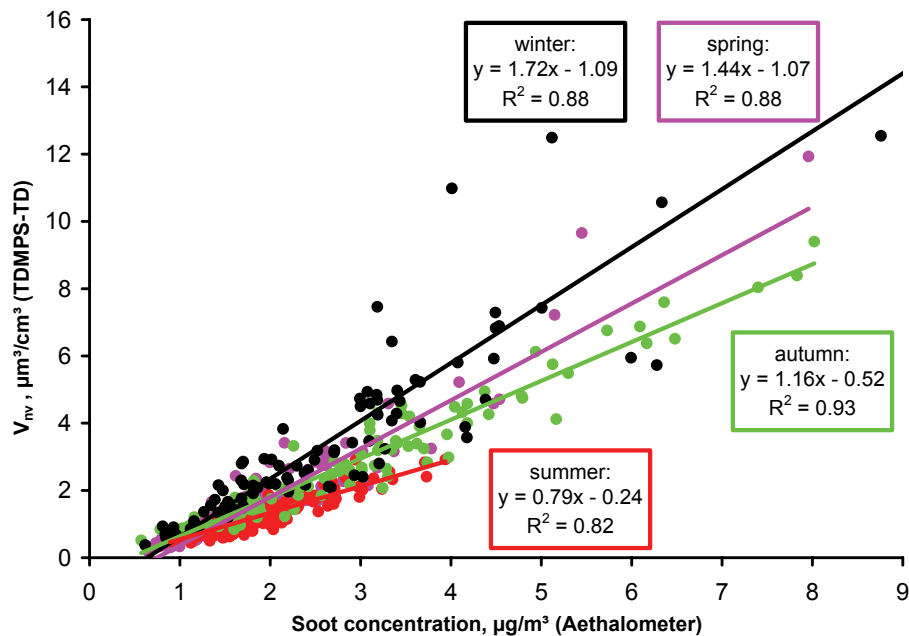


**Fig. 10.** Scatterplot between the soot mass concentration derived from an aethalometer and the non-volatile particle mass concentration ( $D_p < 800$  nm) on the basis of daily averages.

[Title Page](#)[Abstract](#)[Introduction](#)[Conclusions](#)[References](#)[Tables](#)[Figures](#)[◀](#)[▶](#)[◀](#)[▶](#)[Back](#)[Close](#)[Full Screen / Esc](#)[Printer-friendly Version](#)[Interactive Discussion](#)

**Size distributions  
before and after  
volatilisation**

W. Birmili et al.

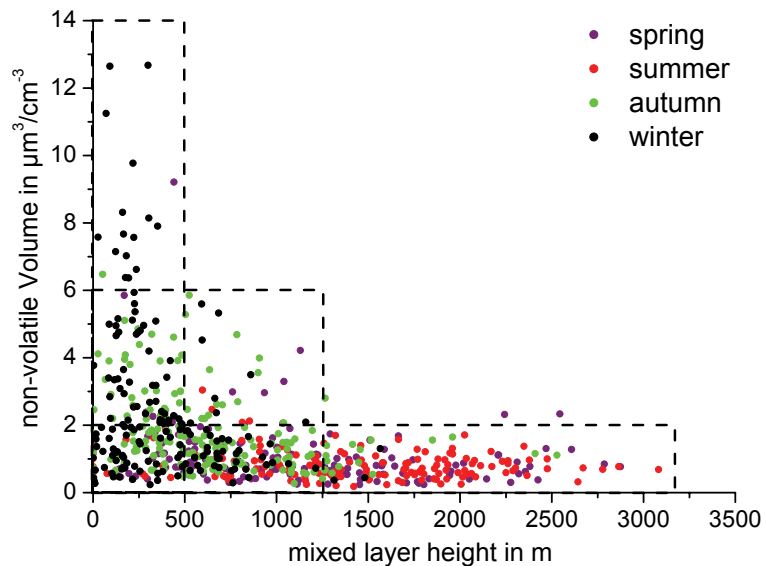


**Fig. 11.** Scatterplot between the mixed layer height and the non-volatile particle volume concentration ( $D_p < 800$  nm). Dashed boxes encircle data clouds.

[Title Page](#)[Abstract](#)[Introduction](#)[Conclusions](#)[References](#)[Tables](#)[Figures](#)[◀](#)[▶](#)[◀](#)[▶](#)[Back](#)[Close](#)[Full Screen / Esc](#)[Printer-friendly Version](#)[Interactive Discussion](#)

**Size distributions  
before and after  
volatilisation**

W. Birmili et al.

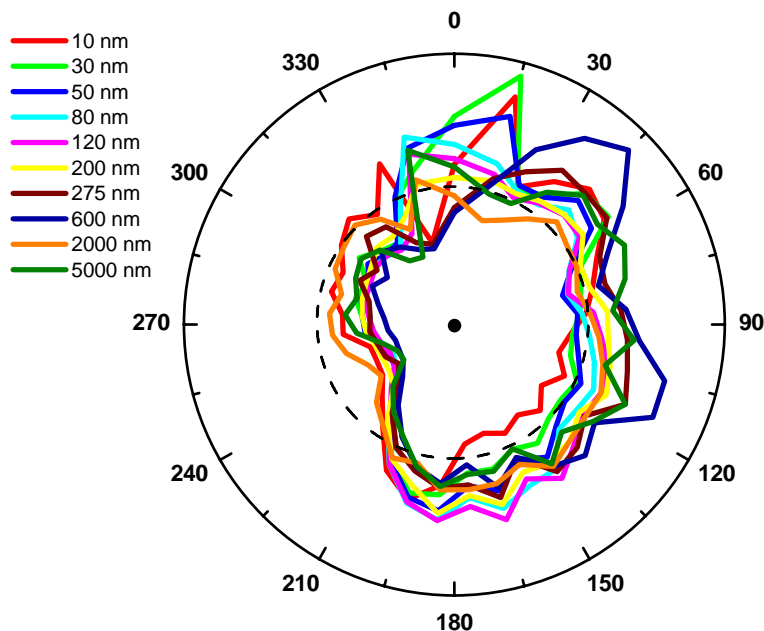


**Fig. 12.** Wind-directional dependence of particle number concentration in Augsburg. Shown is the median concentration for different intervals of wind direction. For better comparability, the number concentration was normalised by the average concentration in each size channel.

[Title Page](#)[Abstract](#)[Introduction](#)[Conclusions](#)[References](#)[Tables](#)[Figures](#)[◀](#)[▶](#)[◀](#)[▶](#)[Back](#)[Close](#)[Full Screen / Esc](#)[Printer-friendly Version](#)[Interactive Discussion](#)

**Size distributions  
before and after  
volatilisation**

W. Birmili et al.

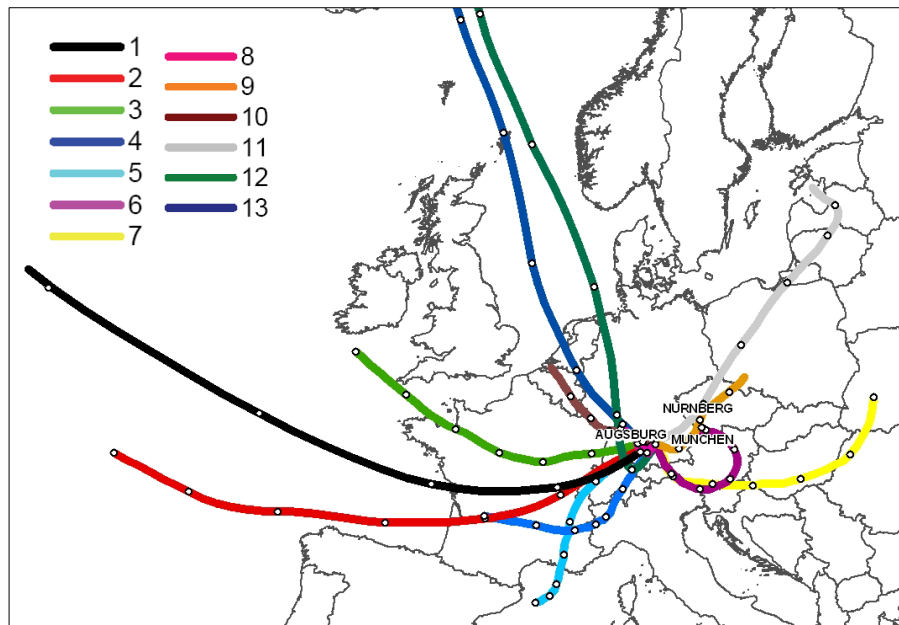


**Fig. 13.** Mean back trajectories of 13 trajectory clusters arriving at Augsburg. The duration of each trajectory is 6 days. One trajectory point corresponds to 24 h.

[Title Page](#)[Abstract](#)[Introduction](#)[Conclusions](#)[References](#)[Tables](#)[Figures](#)[◀](#)[▶](#)[◀](#)[▶](#)[Back](#)[Close](#)[Full Screen / Esc](#)[Printer-friendly Version](#)[Interactive Discussion](#)

**Size distributions  
before and after  
volatilisation**

W. Birmili et al.

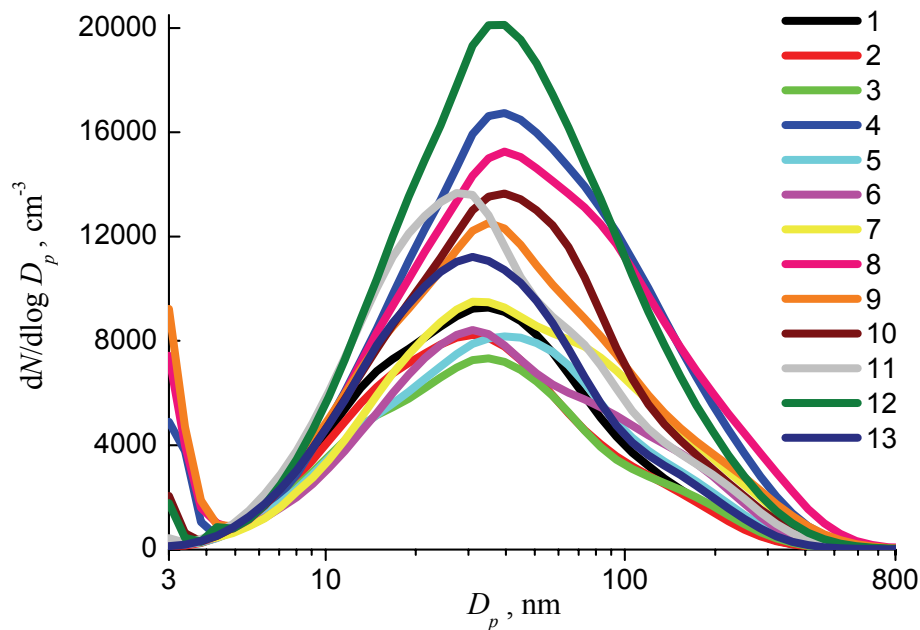


**Fig. 14a.** Mean particle number size distributions for 13 trajectory clusters arriving at Augsburg. Only data during the period 12:00–18:00 LT is considered.

[Title Page](#)[Abstract](#)[Introduction](#)[Conclusions](#)[References](#)[Tables](#)[Figures](#)[◀](#)[▶](#)[◀](#)[▶](#)[Back](#)[Close](#)[Full Screen / Esc](#)[Printer-friendly Version](#)[Interactive Discussion](#)

**Size distributions  
before and after  
volatilisation**

W. Birmili et al.

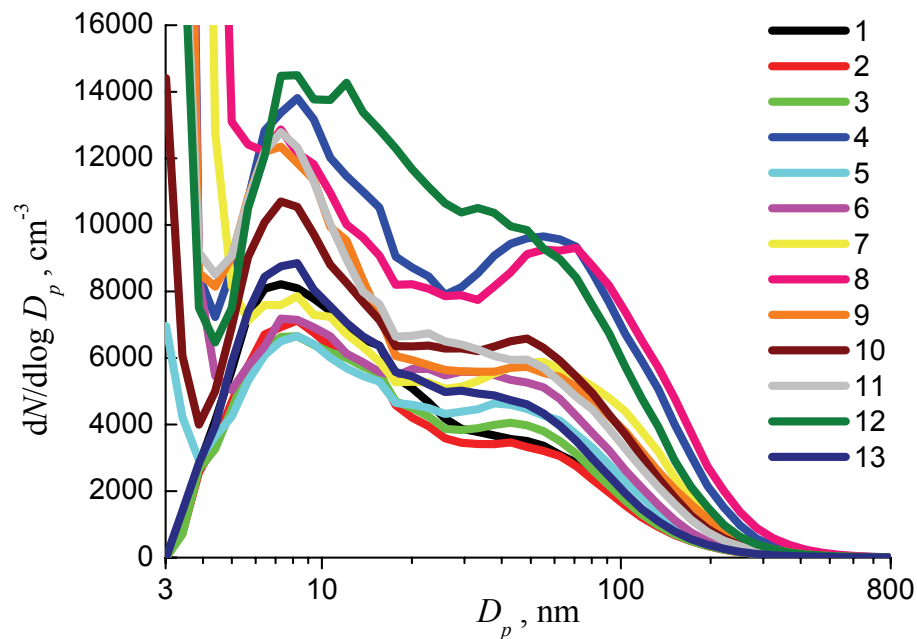


**Fig. 14b.** Mean particle number size distributions after volatilisation at 300°C for 13 trajectory clusters arriving at Augsburg. Only data during the period 12:00–18:00 LT is considered. High concentrations below diameters of 6 nm result from nucleation inside the thermodenuder and are an artifact of the method.

[Title Page](#)[Abstract](#)[Introduction](#)[Conclusions](#)[References](#)[Tables](#)[Figures](#)[◀](#)[▶](#)[◀](#)[▶](#)[Back](#)[Close](#)[Full Screen / Esc](#)[Printer-friendly Version](#)[Interactive Discussion](#)

**Size distributions  
before and after  
volatilisation**

W. Birmili et al.

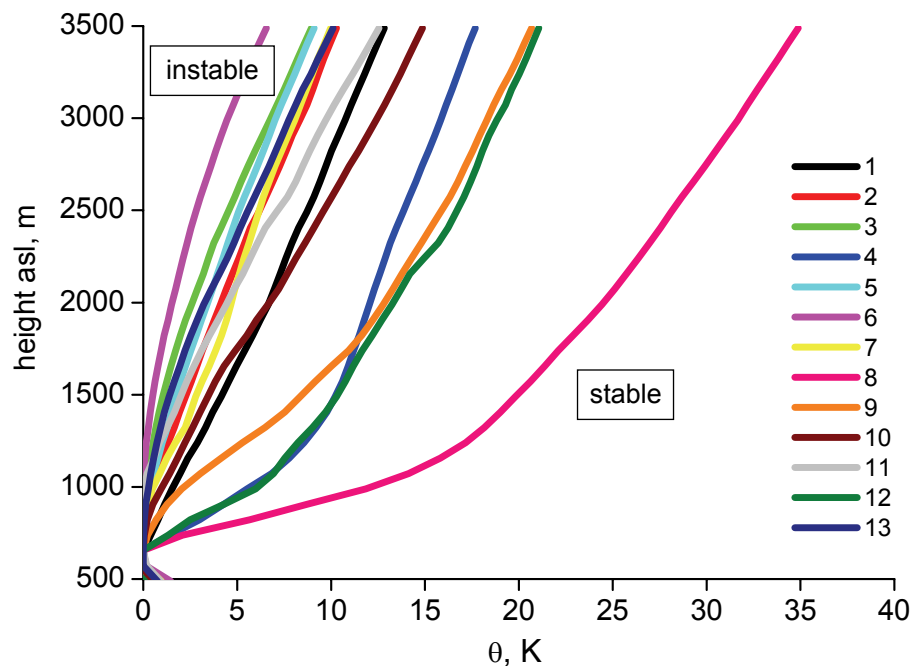


**Fig. 14c.** Mean vertical profiles of pseudopotential temperature ( $\theta$ ) for 13 trajectory clusters arriving at Augsburg. All underlying daily profiles were taken at 13:00 LT at Munich (Ober-schleissheim). For a direct comparability all profiles were normalised to zero at  $h = 650$  m.

Title Page

Abstract

Introduction

Conclusions

References

Tables

Figures

◀

▶

◀

▶

Back

Close

Full Screen / Esc

Printer-friendly Version

Interactive Discussion



Size distributions  
before and after  
volatilisation

W. Birmili et al.

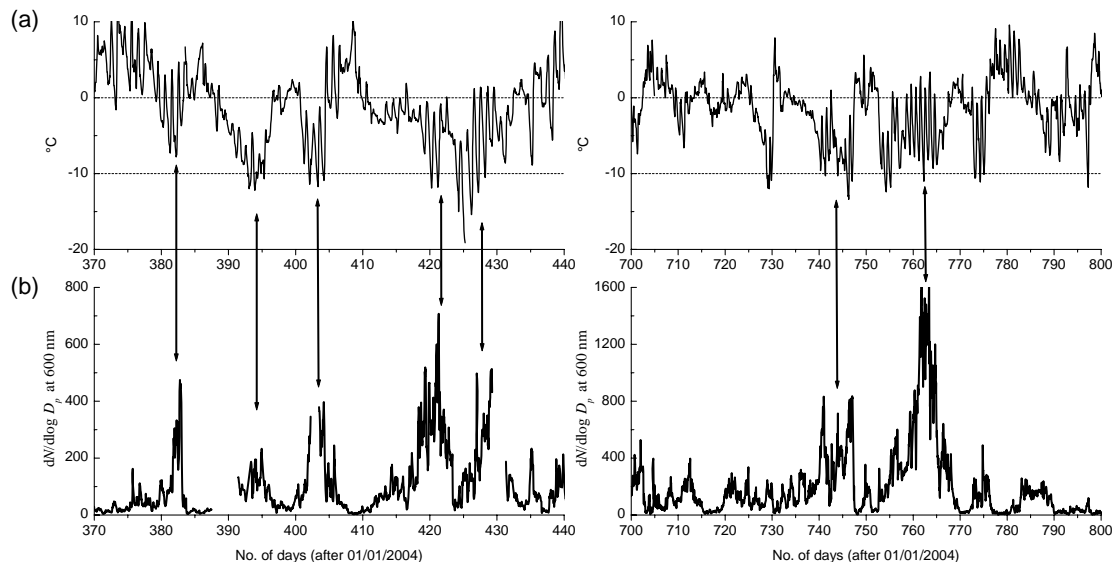


**Fig. 15.** Time history of ambient temperature (a) and the number concentration of 600 nm-particles. The left-hand and right-hand graphs correspond to the winters 2004/2005 and 2005/2006, respectively. Several episodes that show simultaneous high particle concentrations and low temperatures are marked by arrows.

[Title Page](#)[Abstract](#)[Introduction](#)[Conclusions](#)[References](#)[Tables](#)[Figures](#)[◀](#)[▶](#)[◀](#)[▶](#)[Back](#)[Close](#)[Full Screen / Esc](#)[Printer-friendly Version](#)[Interactive Discussion](#)